NASA Technical Memorandum 86221

Three-Dimensional Diffraction of a Plane Wave by a Half-Plane

R. F. Schmidt

JUNE 1985

NASA

TM 86221

THREE-DIMENSIONAL DIFFRACTION OF A PLANE WAVE BY A HALF-PLANE

R. F. Schmidt

June 1985

Goddard Space Flight Center
Greenbelt, Maryland 20771

THREE-DIMENSIONAL DIFFRACTION OF A PLANE WAVE BY A HALF-PLANE

R. F. Schmidt
NASA/Goddard Space Flight Center
Greenbelt, Maryland 20771

ABSTRACT

This document discusses several aspects of the asymptotic Sommerfeld solutions for a diffracting half-plane. The behavior of the E-plane and H-plane solutions for general (two angle-parameter) incidence is explored in the remote shadow, reflection, and illumination regions using the time-average Poynting vector. Field points are also taken on the shadow and reflection boundaries to characterize the behavior of the asymptotic solutions in these special regions. Geometric-optics field transition between adjacent sectors via the arithmetic mean is verified. Numerous sketches are included to assist visualization of the content of the three-dimensional Sommerfeld solutions and clarify some of the notation and conventions introduced in TM 84996 of March 1983. The closed-form field equations discussed in this document provide an analytical basis for comparison with the numerical results of a computer program predicated on the less-restrictive Fresnel-integral approach.

CONTENTS

ILLUSTRATIONS

GLOSSARY OF NOTATION

$\bar{E}_i, \bar{H}_i$	incident electric and magnetic fields (plane-wave)
α, β	azimuthal and polar incidence angles (plane-wave)
k	free-space wave number
(r,θ,z)	local cylindrical coordinates for fences or half-planes
p, q	arguments of the Fresnel integral
a	generic parameter equal to u, v, p, or q
$\bar{S}_i, \bar{S}_r$	incident and reflected rays
$\bar{n}$	surface normal (unit vector)
$<\bar{P}>$	time-average Poynting vector
Re	real part operator
dS	differential area
h_s	slant height of a cone
u	unit designation
c, C	cone, cross-term
Λ	wavefront
δ	deviation from a circular wavefront
λ	wavelength
R	radius
ℓ	stationary distance
N	stationarity criteria

THREE-DIMENSIONAL DIFFRACTION OF A PLANE WAVE BY A HALF-PLANE

INTRODUCTION

This document is a companion paper to TM-84996 of March, 1983 entitled "A Radio-Frequency Analysis of Paraboloidal Antennas Located Near Diffracting Fences." The objective is to explore the asymptotic Sommerfeld solutions presented and derived in the preceding technical memorandum, and to discover in some detail what information they contain. It has been found that the time average Poynting vector is useful in this effort since it is composed of twelve field quantitites: three electric field magnitudes together with their associated phase terms, and the magnetic counterparts to these expressions. It is not necessary to multiply the lengthly expressions of the Sommerfeld solution to obtain the general form of the Poynting vector. Instead, strategic observation points may be selected to obtain simple expressions for fields and power vectors locally. The benefits of this approach include a deeper appreciation of the field equations, a facility for extracting information relating to divergence, wavefront, direction of power-flow, etc., and a useful physical picture of diffraction mechanics of the half-plane illuminated by a plane wave.

A review of the previous TM points out the fact that the overall effort is concerned primarily with diffracted fields at large distances from the half-plane. Computation of the complicated field behavior in the vicinity of the half-plane, such as is illustrated in Ref. 1, p. 576, is not of immediate interest, but will incidentally become available upon the completion of a computer program in which the Fresnel-integral approach is implemented. In fact, only the magnetic fields scattered by the half-plane are essential to the calculation of a perturbation of the sheet-current for a paraboloidal antenna of interest. The present document may therefore be regarded as a self-contained paper pertaining to Sommerfeld's half-plane analysis that also augments TM-84996.

Upon completion of TM-84996 several questions arose concerning coordinate conventions, identification of diffraction regions, singularities of the Sommerfeld solutions, and the divergence and phase gradients exhibited by these fields. Several typographical errors were also discovered in this earlier memorandum. A brief discussion of power flow in terms of the total electromagnetic field and the constituent geometric optics and diffraction fields seemed desirable. These considerations motivated the writing of the second technical memorandum.

PLANE-WAVE SOURCES

The equations given below are found in TM-84996 together with the author's statement that (a) is an azimuthal variation in the equatorial plane, and (β) is a polar variation emanating from the (x,y) plane.

E-plane polarization

$$\overline{E}_i = (-\cos a \sin\beta, -\sin a \sin\beta, \cos\beta)\, e^{-iks} \quad (1)$$

$$\overline{H}_i = (-\sin a, \cos\beta, 0)\, e^{-iks} \quad (2)$$

H-plane polarization

$$\overline{E}_i = (\sin a, -\cos a, 0)\, e^{-iks} \quad (3)$$

$$\overline{H}_i = (-\cos a \sin\beta, -\sin a \sin\beta, \cos\beta)\, e^{-iks} \quad (4)$$

Figure 1 shows the similarity between the angle variables of Born and Wolf and the conventional spherical angles (θ_s, φ_s). Figure 2 shows several plane-wave incidence angles and field components for selected polarization states. Figure 2(a) is relatively easy to visualize, since the angle a is held constant at $\pi/2$ radians. Figure 2(b) is considerably more difficult to visualize since a is specified simply as greater than $\pi/2$ radians. The time-average Poynting vector is identical for both polarization cases. A means of specifying a general polarization state (elliptical) for the incident plane wave is implicit in the preceding and requires only the annexation of an exponential factor for relative phase between the E-plane and H-plane cases given above, and scalar weight factors (ω_1, ω_2) to establish the axial ratio.

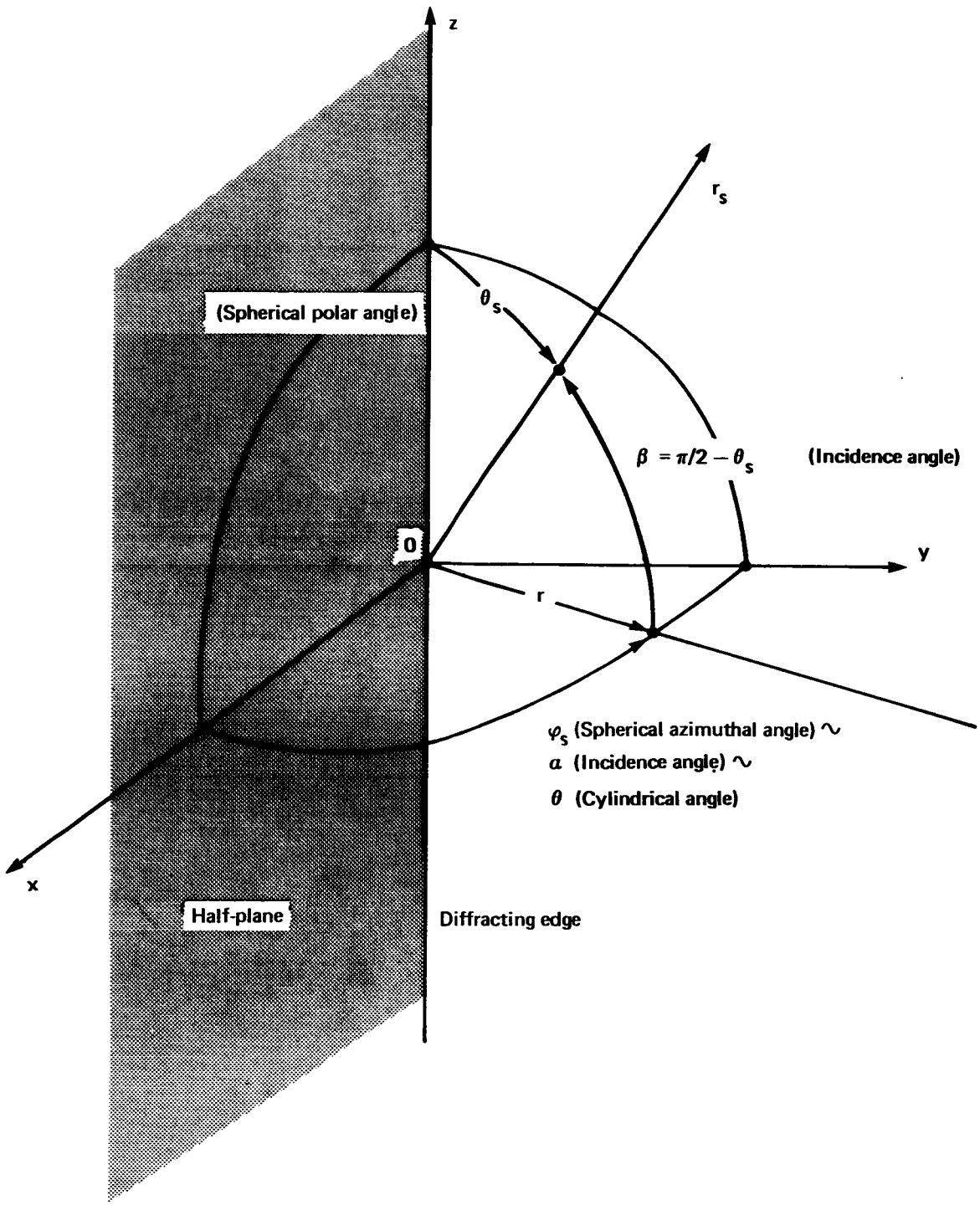

Figure 1. Angle Conventions

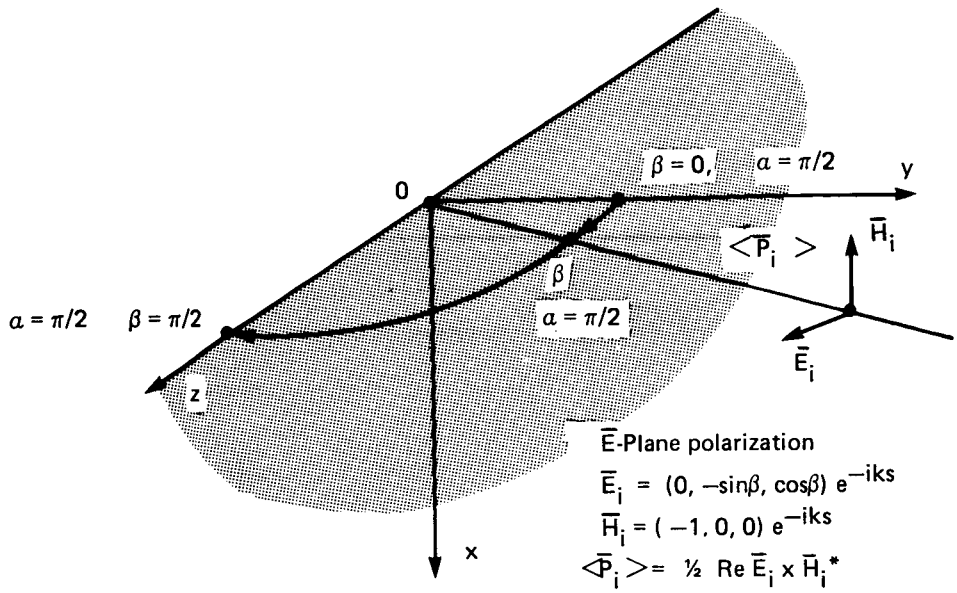

$\overline{E}$-Plane polarization

$\overline{E}_i = (0, -\sin\beta, \cos\beta)\, e^{-iks}$

$\overline{H}_i = (-1, 0, 0)\, e^{-iks}$

$\langle \overline{P}_i \rangle = \frac{1}{2} \operatorname{Re} \overline{E}_i \times \overline{H}_i^*$

$= -\frac{1}{2} (\cos\alpha \cos\beta\, \hat{i} + \cos\beta \sin\alpha\, \hat{j} + \sin\beta\, \hat{k})$

(a)

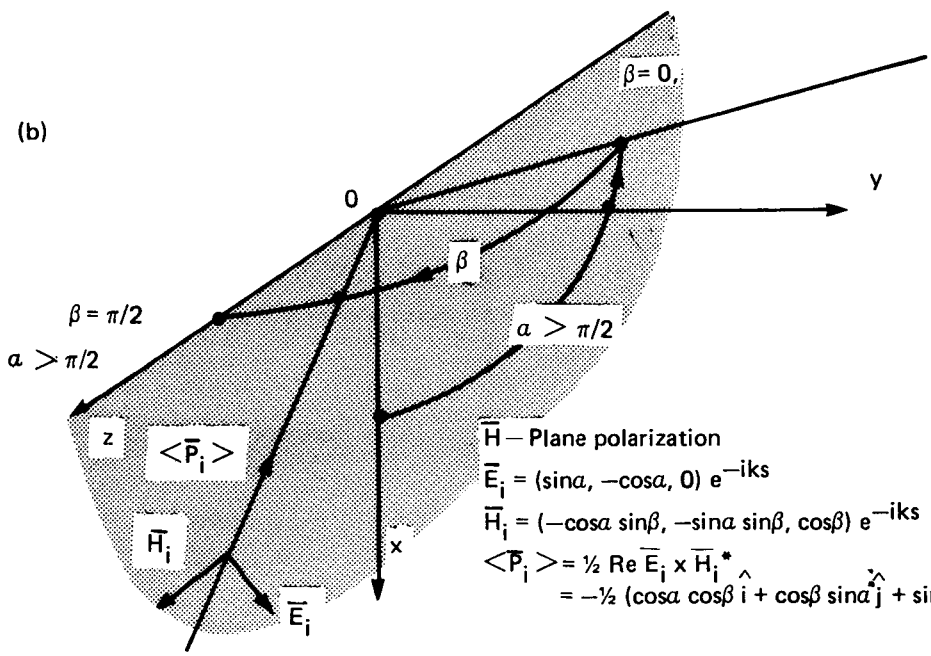

$\overline{H}$ — Plane polarization

$\overline{E}_i = (\sin\alpha, -\cos\alpha, 0)\, e^{-iks}$

$\overline{H}_i = (-\cos\alpha \sin\beta, -\sin\alpha \sin\beta, \cos\beta)\, e^{-iks}$

$\langle \overline{P}_i \rangle = \frac{1}{2} \operatorname{Re} \overline{E}_i \times \overline{H}_i^*$

$= -\frac{1}{2} (\cos\alpha \cos\beta\, \hat{i} + \cos\beta \sin\alpha\, \hat{j} + \sin\beta\, \hat{k})$

Figure 2. Incidence Angles and Field Components

REGIONS AND BOUNDARIES

The plane-wave source angles (α, β) determine regions and boundaries about the diffracting edge of the half-plane. In the text by Born and Wolf three regions and two boundaries are identified in a discussion apparently restricted to a single source angle (α_0). Ref. 1, p. 571, Figure 3 of this document illustrates a plane wave $PW_i(\alpha, \beta)$ incident on a half-plane from a region above the scattering edge. The shadow, reflection, and illumination regions are shown together with the shadow and reflection boundaries.

When applying the asymptotic Sommerfeld field solutions for the three-dimensional case, the arguments

$$a = p = -(2kr\cos\beta)^{1/2}\cos\tfrac{1}{2}(\theta - \alpha) \tag{5}$$

and

$$a = q = -(2kr\cos\beta)^{1/2}\cos\tfrac{1}{2}(\theta + \alpha) \tag{6}$$

must be considered. Ref. 1, p. 572, p. 580. Since

$$G(a) = \sqrt{\pi}\, e^{\pi i/4}\, e^{-ia^2} + \frac{i}{2a} \qquad (a<0)\ , \tag{7}$$

$$G(a) = i/2a \qquad (a>0)\ , \tag{8}$$

and

$$G(a) = \tfrac{1}{2}\sqrt{\pi}\, e^{\pi i/4} \qquad (a=0)\ , \tag{9}$$

it is helpful, when combining the waveforms of the field solutions for analysis, to associate the sign of the argument (a) with particular regions and boundaries. The source angles α, β determine the shadow, reflection, and illumination regions designated SR, RR, IR, respectively, and the shadow and reflection boundaries SB, RB. The angle θ of the cylindrical triad (r, θ, z) of observer coordinates determines the sign of arguments p and q once α has been selected.

Following a two dimensional analysis, Ref. 1, p. 572:

$$\theta = \pi + \alpha_0 \Rightarrow SB \tag{10}$$

and

$$\theta = \pi - \alpha_0 \Rightarrow RB \tag{11}$$

Returning to the three-dimensional case, and substituting the values of θ, above,

$$\theta = \pi + \alpha \Rightarrow p = 0, \quad q > 0 \tag{12}$$

$$\theta = \pi - \alpha \Rightarrow p < 0, \quad q = 0$$

where

$$\alpha \neq 0, \pi \tag{13}$$

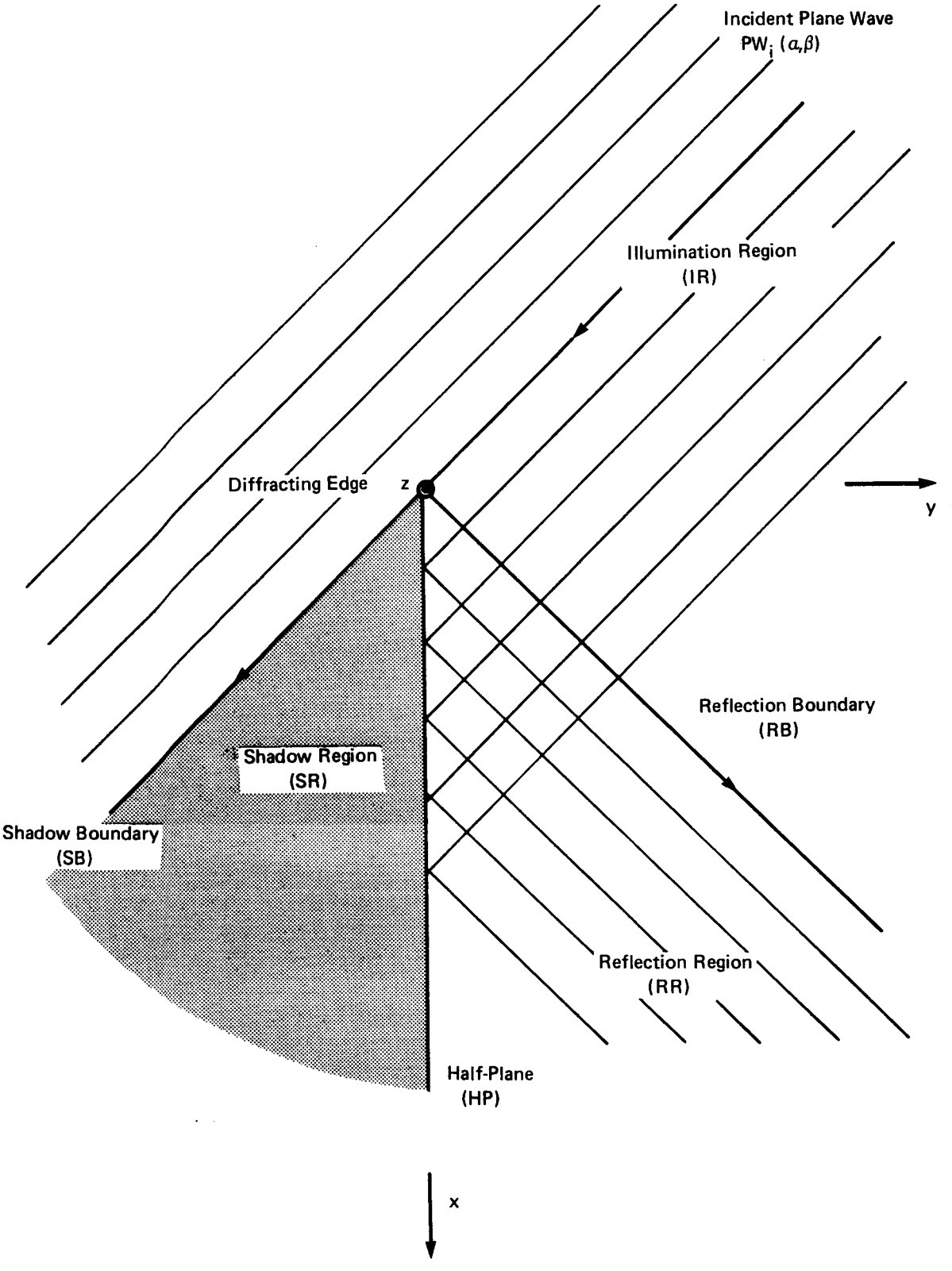

Figure 3. Regions and Boundaries.

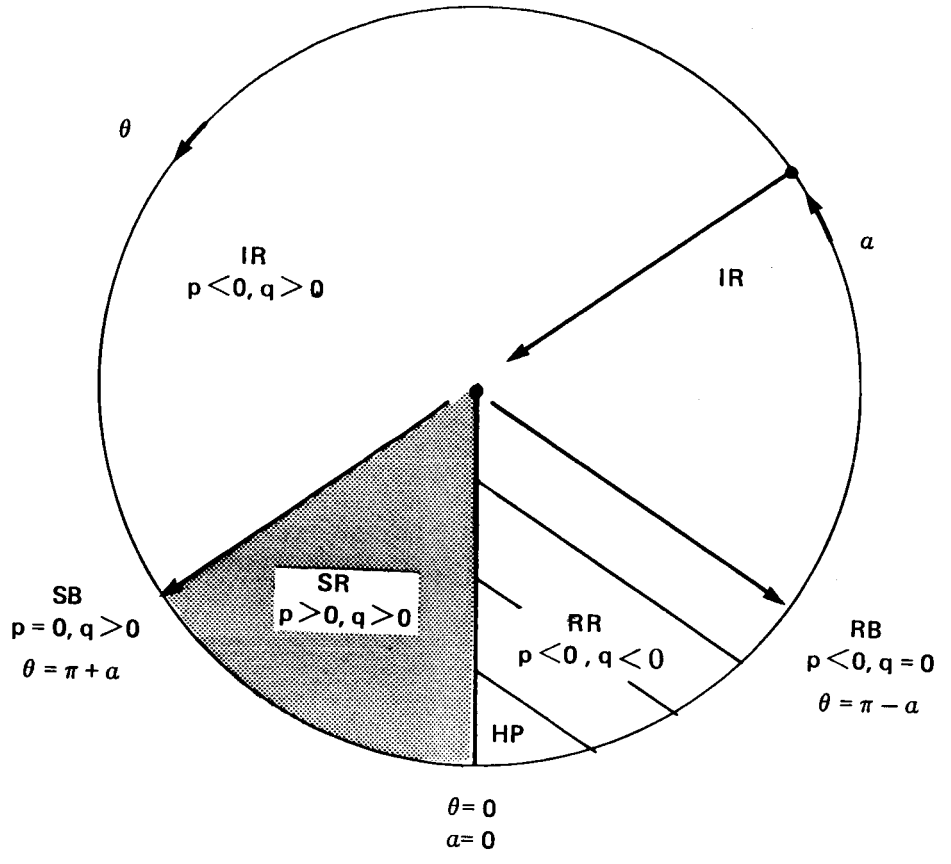

Figure 4. Signs of Arguments p and q.

Further exploration leads to the construction of a mnemonic device, shown as Figure 4.. The transitions in sign for p and q are seen to occur across boundary lines for which the values of p or q equal zero.

An inspection of equations (5) and (6) shows that the signs of p and q are unaffected by the value of angle β ; the value of $\pi/2$ radians is excluded for β here. Since Figure 4 is a function of α alone, but was predicated entirely on equations (10) and (11) of a two dimensional analysis, the possible effect of angle β on the defintion of boundaries and regions is re-examined in a direct manner via a ray trace. The components of a ray representing the incident plane wave are

$$\bar{S}_i = -(\cos\alpha \cos\beta , \sin\alpha \cos\beta , \sin\beta) \tag{14}$$

and the components of the associated reflected ray are

$$\bar{S}_r = \bar{S}_i - 2\,\bar{n}_{HP}\,(\bar{S}_i \cdot \bar{n}_{HP})$$

$$= -(\cos\alpha \cos\beta, -\sin\alpha \cos\beta , \sin\beta) \tag{15}$$

where the components of $\bar{n}_{HP}$ are (0, 1, 0) for the positive normal to the half-plane.

It can now be seen from $\bar{S}_i$ and $\bar{S}_r$ that the angle between SB and HP equals that between RB and HP and is the arc whose tangent is given by the ratio of the magnitude S_y to S_x, independent of angle β. Figure 4 is therefore valid even when β is varied ($-\pi/2 < \beta < \pi/2$). Figures 3 and 4 are cross-sections taken orthogonally to the z-axis. Translations of these figures along z, together with $\bar{S}_i$ and $\bar{S}_r$ give the three-dimensional representation.

SCATTERING FORMULATION (HALF-PLANE)

The asymptotic form of Sommerfeld's half-plane solution is repeated here for convenience. It is noted that TM 84996 contained certain typographical errors which are now corrected. The reader's attention is also directed to the errata section of this memorandum, Appendix. A.

(E-plane Polarization)

$$E_x = -H_y \sin\beta \tag{17}$$

$$E_y = H_x \sin\beta \tag{18}$$

$$E_z = \frac{e^{-\pi i/4}}{\sqrt{\pi}} \cos\beta \; e^{ik(r\cos\beta - z\sin\beta)} \; [G(p) - G(q)] \tag{19}$$

$$H_x = \frac{-e^{-\pi i/4}}{\sqrt{\pi}} e^{ik(r\cos\beta - z\sin\beta)} \left\{ \sin\alpha \, [G(p) + G(q)] + i \left(\frac{2}{kr\cos\beta} \right)^{1/2} \sin\alpha/2 \; \cos\theta/2 \right\} \tag{20}$$

$$H_y = \frac{e^{-\pi i/4}}{\sqrt{\pi}} e^{ik(r\cos\beta - z\sin\beta)} \left\{ \cos\alpha \, [G(p) - G(q)] - i \left(\frac{2}{kr\cos\beta} \right)^{1/2} \sin\alpha/2 \sin\theta/2 \right\} \tag{21}$$

$$H_z \equiv 0 \tag{22}$$

(H-plane Polarization)

$$E_x = \frac{e^{-\pi i/4}}{\sqrt{\pi}} e^{ik(r\cos\beta - z\sin\beta)} \left\{ \sin\alpha \, [G(p) - G(q)] \oplus i \left(\frac{2}{kr\cos\beta} \right)^{1/2} \cos\alpha/2 \sin\theta/2 \right\} \tag{23}$$

$$E_y = \frac{-e^{-\pi i/4}}{\sqrt{\pi}} e^{ik(r\cos\beta - z\sin\beta)} \left\{ \cos\alpha\,[G(p) + G(q)] \right.$$

$$\left. \oplus\, i\left(\frac{2}{kr\cos\beta}\right)^{1/2} \cos\alpha/2\,\cos\theta/2 \right\} \tag{24}$$

$$E_z \equiv 0 \tag{25}$$

$$H_x = E_y \sin\beta \tag{26}$$

$$H_y = -E_x \sin\beta \tag{27}$$

$$H_z = \frac{e^{-\pi i/4}}{\sqrt{\pi}} \cos\beta\; e^{ik(r\cos\beta - z\sin\beta)}[G(p) + G(q)] \tag{28}$$

Note:

The circled signs preceding the imaginary terms of equations (23) and (24), above, were obtained in a derivationof TM-84996 and are different from

Ref. 1, 2nd ed. (–i), (–i)

Ref. 1, 6th Ed. (–i), (+i) ,

respectively. Discussion of this issue is deferred until after the E-plane polarization case has been treated in detail.

An inspection of the Sommerfeld asymptotic solution shows that the total field is comprised of plane wave and cylindrical wave constituents. The time-average Poynting vector will be predicated on the total electric and magnetic fields, respecting amplitude, phase, and polarization. The constituents themselves have interesting properties with regard to divergence, phase gradient, direction of propagation, singularities, etc., and are examined before composition of the general Poynting vector predicated on total fields.

E-PLANE POLARIZATION ($\alpha = \pi/2,\ \beta = 0$)

The E-plane asymptotic solution is considered for a special case of normal incidence ($\alpha = \pi/2$, $\beta = 0$) with the observer initially at

$$(r,\theta,z) = (r,\pi,0) \tag{29}$$

under the assumption that

$$kr\cos\beta = kr >> 1 \quad . \tag{30}$$

Figure 5 shows that the field point lies in the illumination region IR and, using Figure 4, $p < 0$, $q > 0$ is anticipated and verified:

$$a = p = -(2kr\cos\beta)^{1/2}\cos\tfrac{1}{2}(\theta - \alpha) = -(2kr)^{1/2}\sqrt{2}/2 = -(kr)^{1/2} < 0. \tag{31}$$

$$a = q = -(2kr\cos\beta)^{1/2}\cos\tfrac{1}{2}(\theta + \alpha) = (2kr)^{1/2}\sqrt{2}/2\ (kr)^{1/2} > 0. \tag{32}$$

Using the preceding arguments in equations (7) and (8),

$$G(p) = \sqrt{\pi}\ e^{\pi i/4}\ e^{-ikr} - \frac{i}{2(kr)^{1/2}} \quad , \tag{33}$$

and

$$G(q) = \frac{i}{2(kr)^{1/2}} \quad . \tag{34}$$

The geometric optics and diffraction fields may now be identified for equations (17) through (22).

$$E_z = 1 - i\,\frac{e^{-\pi i/4}}{\sqrt{\pi}}\ \frac{e^{ikr}}{(kr)^{1/2}} \tag{35}$$

$$H_x = -1 \tag{36}$$

$$H_y = -i\,\frac{e^{-\pi i/4}}{\sqrt{\pi}}\ \frac{e^{ikr}}{(kr)^{1/2}} \tag{37}$$

$$E_x = E_y = H_z = 0. \tag{38}$$

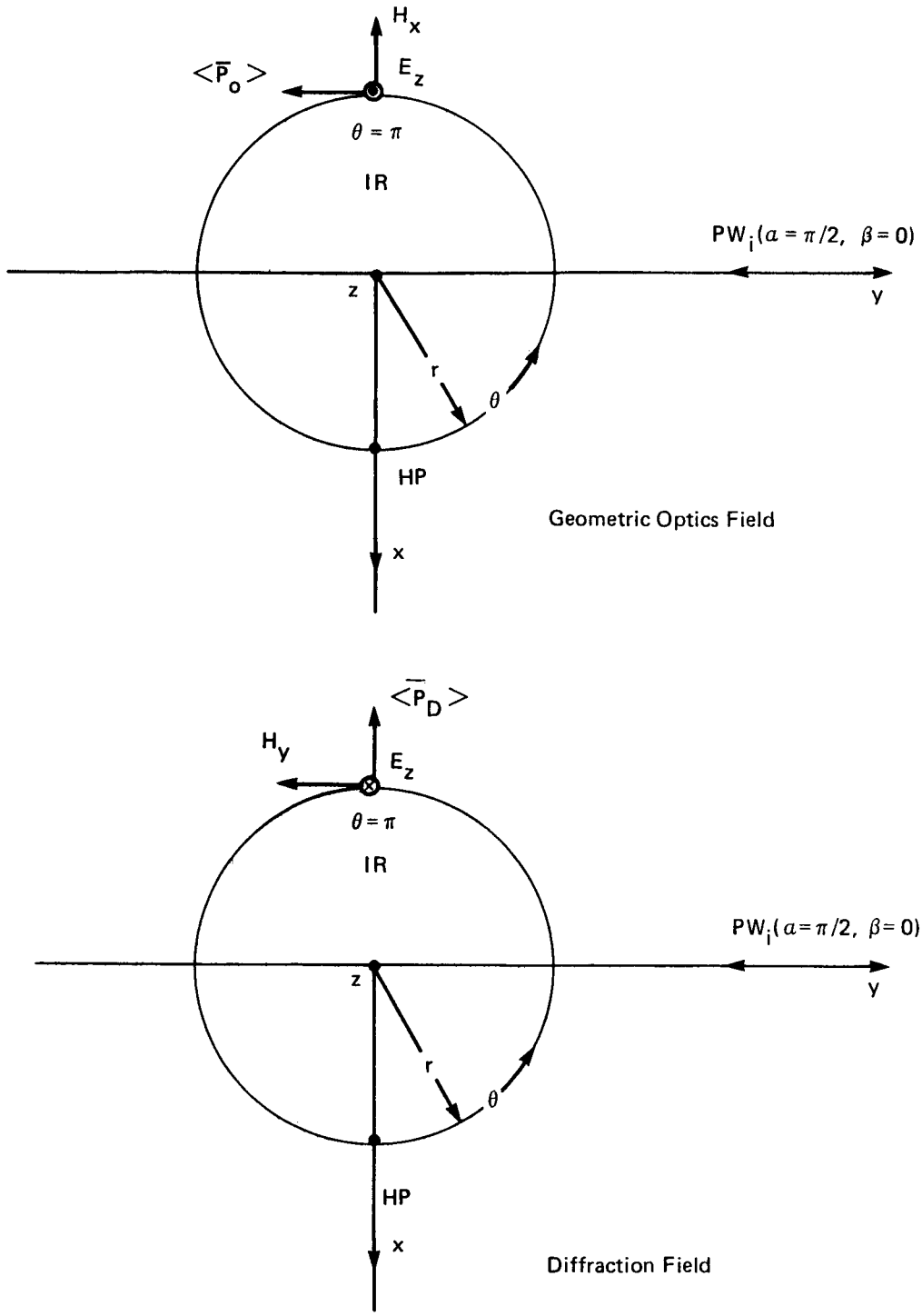

Figure 5. Geometric Optics and Diffraction Fields (E-Plane Polarization)
$a = \pi/2,\ \beta = 0,\ \theta = \pi$

The time-average Poynting vector, using the total fields, is

$$<\bar{P}> = \tfrac{1}{2}\,\mathrm{Re}\,\bar{E}\times\bar{H}^{*} = \tfrac{1}{2}\,\mathrm{Re}\,[\hat{i}(E_yH_z^{*} - E_zH_y^{*}) + \hat{j}(E_zH_x^{*} - E_xH_z^{*}) + \hat{k}\,(E_xH_y^{*} - E_yH_x^{*})] \quad (39)$$

which reduces to

$$<\bar{P}> = \tfrac{1}{2}\mathrm{Re}\,[-\hat{i}\,E_zH_y^{*} + \hat{j}\,E_zH_x^{*}] = <\bar{P}_D(r^{-1})> + <\bar{P}_o(r^{o})> + <\bar{P}_C(r^{-1/2})>$$

$$= \tfrac{1}{2}\left[\frac{-\hat{i}}{\pi\,kr} \quad -\hat{j}\right] + 0 <\bar{P}_C\,(r^{-1/2})>, \quad (40)$$

and is illustrated in Figure 5.

When the observer position is

$$(r, \theta, z) = (r, 7\pi/4, 0) \quad (41)$$

the field point lies in the shadow region SR and, using Figure 4, $p > 0$, $q > 0$ is anticipated and verified:

$$a = p = -(2kr\cos\beta)^{1/2}\cos\tfrac{1}{2}(\theta - a) = -(2kr)^{1/2}\cos 5\pi/8 = .383(2kr)^{1/2} > 0, \quad (42)$$

$$a = q = -(2kr\cos\beta)^{1/2}\cos\tfrac{1}{2}(\theta + a) = -(2kr)^{1/2}\cos 9\pi/8 = .924(2kr)^{1/2} > 0\,. \quad (43)$$

Here

$$G(p) = \frac{1.31\,i}{(2kr)^{1/2}} \quad (44)$$

$$G(q) = \frac{.541\,i}{(2kr)^{1/2}} \quad (45)$$

and

$$E_z = \frac{.543\,i\,e^{-\pi i/4}\;e^{ikr}}{\sqrt{\pi}\qquad (kr)^{1/2}} \quad (46)$$

$$H_x = \frac{-e^{-\pi i/4}}{\sqrt{\pi}}\,e^{ikr}\left[\frac{1.31\,i}{(kr)^{1/2}} - \frac{.926\,i}{(kr)^{1/2}}\right] = \frac{-.384\,i\,e^{-\pi i/4}e^{ikr}}{\sqrt{\pi}\;(kr)^{1/2}} \quad (47)$$

$$H_y = \frac{-.383i\,e^{-\pi i/4}\;e^{ikr}}{\sqrt{\pi}\qquad (kr)^{1/2}} \quad (48)$$

$$E_x = E_y = H_z = 0 . \tag{49}$$

The Poynting vector reduces to

$$<\bar{P}> = \tfrac{1}{2}\,\mathrm{Re}\,[-\hat{i}\,E_z H_y^* + \hat{j}\,E_z H_x^*] = <\bar{P}_D(r^{-1})> + <\bar{P}_o(r^o)> + <\bar{P}_C(r^{-1/2})>$$

$$= \tfrac{1}{2}\left[\frac{.208\,\hat{i}}{\pi kr} - \frac{.209\,\hat{j}}{\pi kr}\right] + 0 <\bar{P}_o(r^o) + 0 <\bar{P}_C(r^{-1/2})> \tag{50}$$

with a small roundoff error, and is illustrated in Figure 6.

When the observer position is

$$(r,\theta, z) = (r, \pi/4, 0) \tag{51}$$

the field point lies in the reflection region RR and, using Figure 4, $p<0$, $q<0$ is anticipated and verified:

$$a = p = -(2kr\cos\beta)^{1/2}\cos\tfrac{1}{2}(\theta - \alpha) = -.924\,(2kr)^{1/2} < 0 \quad , \tag{52}$$

$$a = q = -(2kr\cos\beta)^{1/2}\cos\tfrac{1}{2}(\theta + \alpha) = -.383\,(2kr)^{1/2} < 0 \quad . \tag{53}$$

Here

$$G(p) = \sqrt{\pi}\,e^{\pi i/4}\,e^{-1.71kr\,i} - \frac{.383\,i}{(kr)^{1/2}} \tag{54}$$

$$G(q) = \sqrt{\pi}\,e^{\pi i/4}\,e^{-.293kr\,i} - \frac{.923\,i}{(kr)^{1/2}} \tag{55}$$

and

$$E_z = \frac{e^{-\pi i/4}}{\sqrt{\pi}}\,e^{ikr}\left[\sqrt{\pi}\,e^{\pi i/4}\,(e^{-1.71kr\,i} - e^{-.293kr\,i}) + \frac{.540\,i}{(kr)^{1/2}}\right] \tag{56}$$

$$H_x = \frac{-e^{-\pi i/4}}{\sqrt{\pi}}\,e^{ikr}\left[\sqrt{\pi}\,e^{\pi i/4}\,(e^{-1.71kr\,i} + e^{-.293kr\,i}) - \frac{.383\,i}{(kr)^{1/2}}\right] \tag{57}$$

$$H_y = \frac{-.383\,i\,e^{-\pi i/4}\,e^{ikr}}{\sqrt{\pi}\,(kr)^{1/2}} \tag{58}$$

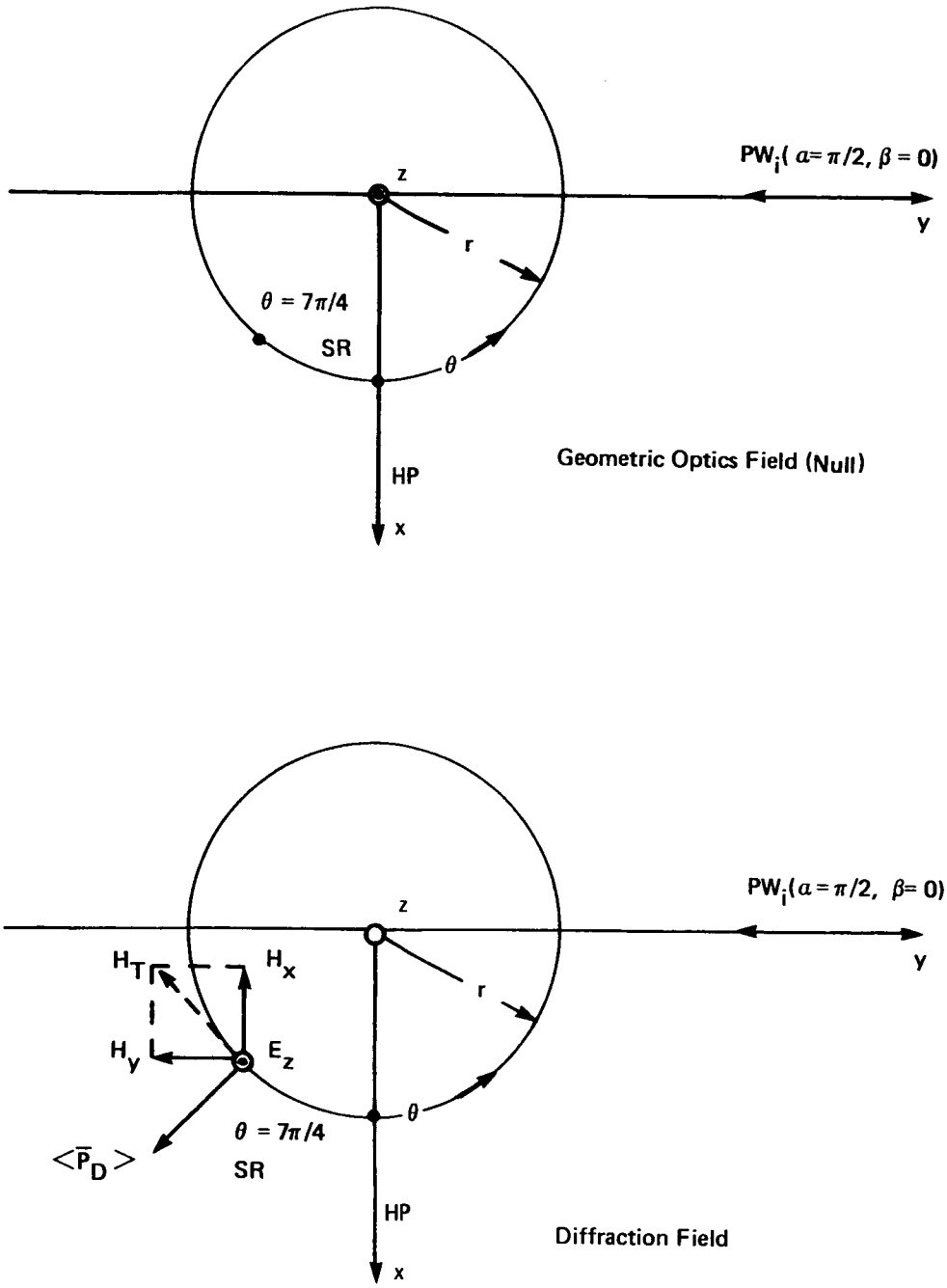

Figure 6. Geometric Optics and Diffraction Fields (E-Plane Polarization)
$\alpha = \pi/2$, $\beta = 0$, $\theta = 7\pi/4$

$$E_x = E_y = H_z = 0 \ . \tag{59}$$

The Poynting vector reduces to

$$\langle \bar{P} \rangle = \tfrac{1}{2} \mathrm{Re} \left[-\hat{i} E_z H_y^* + \hat{j} E_z H_x^* \right] = \langle \bar{P}_D(r^{-1}) \rangle + \langle \bar{P}_o(r^o) \rangle + \langle \bar{P}_C(r^{-1/2}) \rangle$$

$$= \tfrac{1}{2} \left[\frac{.207 \hat{i}}{\pi kr} + \frac{.207 \hat{j}}{\pi kr} \right] + 0 \langle \bar{P}_o(r^o) \rangle + \langle \bar{P}_C(r^{-1/2}) \rangle \tag{60}$$

and is illustrated in Figure 7.

Equation (60) requires some discussion. In Figures 5, 6, 7 the diffracted fields and geometric optics fields are indicated. The accompanying Poynting vectors $\langle \bar{P}_o \rangle$ and $\langle \bar{P}_D \rangle$ may be associated with zero, one, or two geometric optics plane waves, and the diffracted cylindrical wave, respectively. In the IR of Figure 5 both $\langle \bar{P}_D \rangle$ and $\langle \bar{P}_o \rangle$ are non-vanishing. In the SR of Figure 6 the $\langle \bar{P}_D \rangle$ is non-vanishing, but the $\langle \bar{P}_o \rangle$ equals zero. In the RR of Figure 7 an examination of the Poynting vector $\langle \bar{P}_o \rangle$ that incorporates the total electric and magnetic fields shows that power-density at a point diverges (vacuously) as r^o, and also as r^{-1} and $r^{-1/2}$.

The vanishing of the $\langle \bar{P}_o \rangle$ term for Figure 7 is apparent from two considerations. Equations (56) and (57) show that the geometric optics field in the RR is due to an incident and a reflected plane wave. Considering the $\langle \bar{P}_o \rangle$ of these oppositely directed waves ($\alpha = \pi/2, \beta = 0$), the net power flow should be zero. An alternative approach is available via the definition of the time-average Poynting vector:

$$\langle \bar{P}_o \rangle = \tfrac{1}{2} \mathrm{Re}\, \bar{E}_z \times \bar{H}_x^* = 0 \tag{61}$$

since

$$(e^{-A} - e^{-i B})(e^{i A} + e^{i B}) = -2 i \sin(A - B) \tag{62}$$

is purely imaginary. The factors $e^{-\pi i/4}$, $-e^{-\pi i/4}$, e^{ikr} are taken into account.

Equations (54) and (55) may be rewritten to display the geometric optics fields more clearly by writing

$$p^2 = 2kr \cos\beta \cos^2 \tfrac{1}{2}(\theta - \alpha) = kr \cos\beta \, [1 + \cos(\theta - \alpha)] \tag{63}$$

and

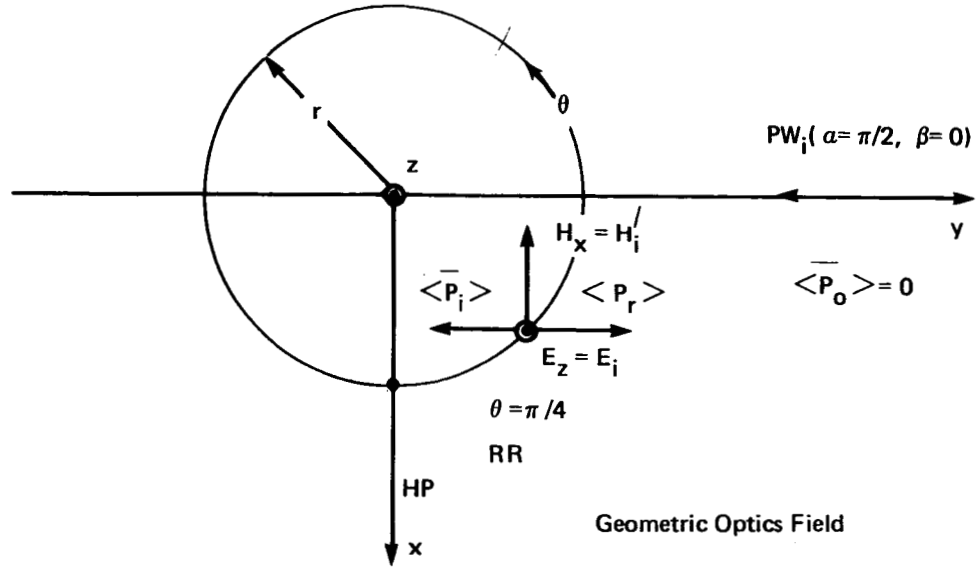

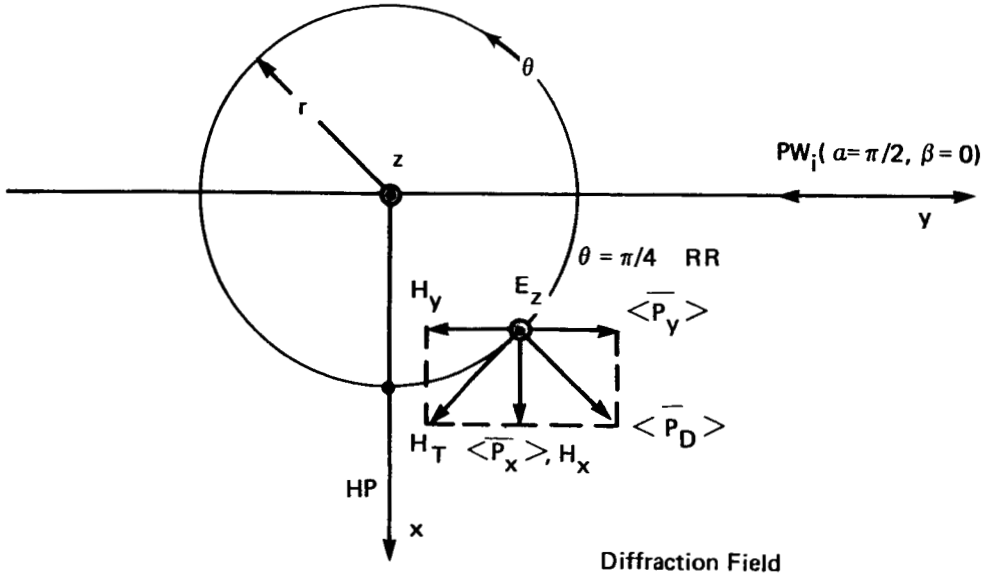

Figure 7. Geometric Optics and Diffraction Fields (E-Plane Polarization)
$\alpha = \pi/2,\ \beta = 0,\ \theta = \pi/4$

$$q^2 = 2kr\cos\beta\cos^2 \tfrac{1}{2}(\theta + a) = kr\cos\beta\ [1 + \cos(\theta + a)]\ . \tag{64}$$

Then, in the expressions for G(p) and G(q),

$$e^{-ia^2} = e^{-ip^2} = e^{ikr\cos\beta}\ e^{-ikr\cos\beta\cos(\theta - a)} \tag{65}$$

and

$$e^{-ia^2} = e^{-iq^2} = e^{-ikr\cos\beta}\ e^{-ikr\cos\beta\cos(\theta + a)}\ . \tag{66}$$

In Figure 7, β equals zero, and the incident and reflected plane waves are identified. See Ref. 1, p. 572. Only the incident plane wave components are illustrated since the reflected plane wave components are similar except for phase factors. The electric and magnetic boundary conditions are seen to be satisfied here for θ equals $\pi/4$ radians and r equals zero and, more generally, along the half plane for θ equals zero and any value of r for both E-plane and H-plane solutions.

The $< \overline{P}_D(r^{-1}) >$ term of equation (60) evolves via the cylindrical electric field term of equation (56) and the cylindrical magnetic field terms of equations (57) and (58). For the parameters of the present example it happens that the $\hat{i}$ and $\hat{j}$ components of $< \overline{P}_D >$ are equal, and the direction of the power-density vector is orthogonal to the cylindrical wavefront as shown in Figure 7.

The $< \overline{P}_C(r^{-1/2}) >$ term of equation (60) is a result of two cross-products, equations (56) and (57), leading to a $(r^{-1/2})$ law of power divergence unlike that of geometric optics (r^0) or diffraction (r^{-1}). In Figure 7 the complicated power-flow in the SR must be due to the $< \overline{P}_C >$ term since $< \overline{P}_o >$ equals zero, and $< \overline{P}_D >$ is a simple power term associated with a cylindrical wave. (Ref. 1, pp.576, 577, maps H-plane polarization fields and power flow.) It is noted that both H_x^* and H_y^*, interacting with E_z, give rise to cross terms that diverge as $(r^{-1/2})$, but the operation (½ Re) must be taken into account.

When the observer position is

$$(r, \theta, z) = (r,\ 3\pi/2,\ z) \tag{67}$$

the field point lies on the shadow boundary SB and, using Figure 4, $p = 0$, $q > 0$ is anticipated and verified:

$$a = p = -(2kr\cos\beta)^{1/2}\cos\tfrac{1}{2}(\theta - a) = 0 \tag{68}$$

$$a = q = -(2kr\cos\beta)^{1/2}\cos\tfrac{1}{2}(\theta + a)^{1/2} = (2kr)^{1/2} > 0\ . \tag{69}$$

Here

$$G(p) = \tfrac{1}{2}\sqrt{\pi}\, e^{\pi i/4} \tag{70}$$

$$G(q) = \frac{i}{2(2kr)^{1/2}} \tag{71}$$

and

$$E_z = \frac{e^{-\pi i/4}}{\sqrt{\pi}}\, e^{ikr} \left[\tfrac{1}{2}\sqrt{\pi}\, e^{\pi i/4} - \frac{i}{2\sqrt{2}\,(kr)^{1/2}} \right] \tag{72}$$

$$H_x = \frac{-e^{-\pi i/4}}{\sqrt{\pi}}\, e^{ikr} \left[\tfrac{1}{2}\sqrt{\pi}\, e^{\pi i/4} - \frac{i}{2\sqrt{2}\,(kr)^{1/2}} \right] \tag{73}$$

$$H_y = \frac{e^{-\pi i/4}}{\sqrt{\pi}} e^{ikr} \left[\frac{-i}{\sqrt{2}\,(kr)^{1/2}} \right] \tag{74}$$

$$E_x = E_y = H_z = 0\,. \tag{75}$$

The Poynting vector reduces to

$$\langle \bar{P} \rangle = \tfrac{1}{2}\,\mathrm{Re}\,[-\hat{i}\,E_z H_y^* + \hat{j}\,E_z H_x^*] = \langle \bar{P}_D(r^{-1}) \rangle + \langle \bar{P}_o(r^o) \rangle + \langle \bar{P}_C(r^{-1/2}) \rangle$$

$$= \tfrac{1}{2} \left[\frac{-\hat{i}}{4\pi kr} - \frac{\hat{j}}{8\pi kr} - \frac{\hat{j}}{4} \right] + \langle \bar{P}_C(r^{-1/2}) \rangle \tag{76}$$

and is illustrated in Figure 8.

The diffracted Poynting vector $\langle \bar{P}_D \rangle$ is no longer orthogonal to the cylindrical wavefront for the present evaluation on the SB even though the exact form of G(p), equation (70), was used. See Ref. 1, p. 571, p. 573. It appears that the Fresnel integral approach should be employed here. Additional insight is provided by studying the behavior of the asymptotic solution as θ approaches the SB from the IR. (See Figures 9 and 10 and subsequent discussion.)

Although the asymptotic solution leads to a doubtful result on the SB regarding the diffracted wave, the geometrical optics result is reliable. From equation (72),

$$E_z(r^o) = \tfrac{1}{2}\, e^{ikr} \tag{77}$$

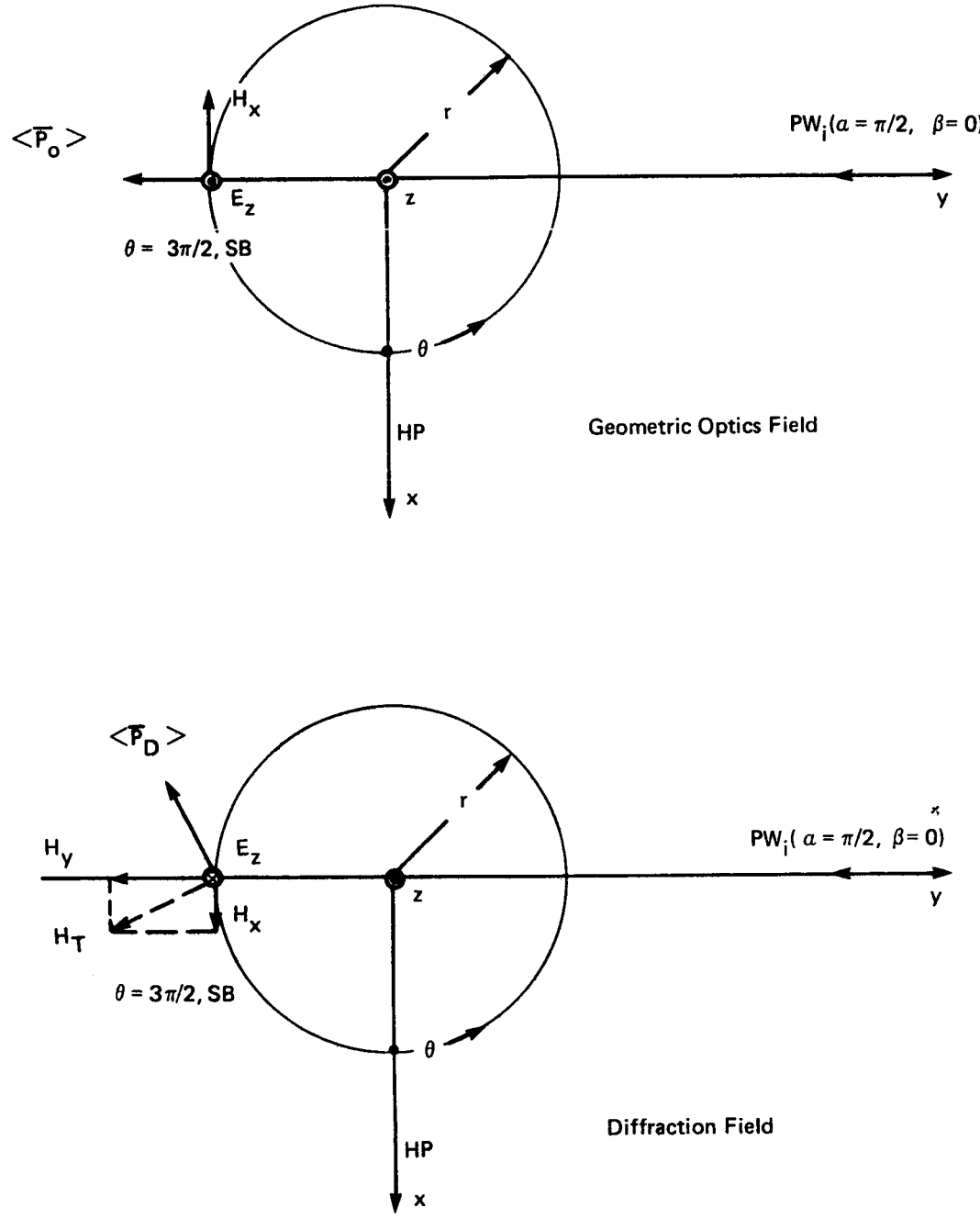

Figure 8. Geometric Optics and Diffraction Fields (E-Plane Polarization)
$\alpha = \pi/2,\ \beta = 0,\ \theta = 3\pi/2$

which is the arithmetic mean of values on either side of the shadow boundary:

$$\text{A.M.} = \tfrac{1}{2}\left(\underset{\text{IR}}{e^{-ikr\cos\beta\cos(\theta-\alpha)}} + \underset{\text{SR}}{0} \right) . \tag{78}$$

Here the values of α,β , and θ are $\pi/2$, 0, and $3\pi/2$, respectively.

When the observer position is

$$(r,\theta, z) = (r, 5\pi/4, z) \tag{79}$$

the field point lies in the illumination region IR and, using Figure 4, $p < 0, q > 0$ is anticipated and verified:

$$a = p = -(2kr\cos\beta)^{1/2}\cos\tfrac{1}{2}(\theta-\alpha) = -.383(2kr)^{1/2} < 0 \tag{80}$$

$$a = q = -(2kr\cos\beta)^{1/2}\cos\tfrac{1}{2}(\theta+\alpha) = .924(2kr)^{1/2} > 0 . \tag{81}$$

Here

$$G(p) = \sqrt{\pi}\, e^{\pi i/4}\ e^{-.293\,kr\,i} - \frac{.923\,i}{(kr)^{1/2}} \tag{82}$$

$$G(q) = \frac{.383\,i}{(kr)^{1/2}} \tag{83}$$

and

$$E_z = \frac{e^{-\pi i/4}}{\sqrt{\pi}}\, e^{ikr}\left[\sqrt{\pi}\, e^{\pi i/4}\ e^{-.293\,kr\,i} - \frac{1.31\,i}{(kr)^{1/2}}\right] \tag{84}$$

$$H_x = \frac{-e^{-\pi i/4}}{\sqrt{\pi}}\, e^{ikr}\left[\sqrt{\pi}\, e^{\pi i/4}\ e^{-.293\,kr\,i} - \frac{.923\,i}{(kr)^{1/2}}\right] \tag{85}$$

$$H_y = \frac{-.924\,i\, e^{-\pi i/4}\, e^{ikr}}{\sqrt{\pi}\,(kr)^{1/2}} \tag{86}$$

$$E_x = E_y = E_z = 0 . \tag{87}$$

The Poynting vector reduces to

$$<\bar{P}> = \tfrac{1}{2}\,\mathrm{Re}\,[\,-\hat{i}\,E_z H_y^* + \hat{j}\,E_z H_x^*\,] = <\bar{P}_D(r^{-1})> + <\bar{P}_o(r^o)> + <\bar{P}_C(r^{-1/2})>$$

$$= \tfrac{1}{2}\left[\frac{-1.21\,\hat{i}}{\pi kr} - \frac{1.21\,\hat{j}}{\pi kr} - \hat{j}\right] + <\bar{P}_C(r^{-1/2})>\,. \tag{88}$$

and is illustrated in Figure 9.

When the observer position is

$$(r, \theta\,.\,z) = (r,\, 11\pi/8,\, z) \tag{89}$$

the field point lies in the illumination region IR, but close to the shadow boundary SB and using Figure 4, $p<0$, $q>0$ is anticipated and verified.

$$a = p = -(2kr\,\cos\beta)^{1/2}\cos\tfrac{1}{2}(\theta - \alpha) = -.195\,(2kr)^{1/2} < 0 \tag{90}$$

$$a = q = -(2kr\,\cos\beta)^{1/2}\cos\tfrac{1}{2}(\theta + \alpha) = .981\,(2kr)^{1/2} > 0\,. \tag{91}$$

Here

$$G(p) = \sqrt{\pi}\,e^{\pi i/4}\;e^{-.076\,kr\,i} - \frac{1.81\,i}{(kr)^{1/2}} \tag{92}$$

$$G(q) = \frac{.360\,i}{(kr)^{1/2}} \tag{93}$$

and

$$E_z = \frac{e^{-\pi i/4}}{\sqrt{\pi}}\,e^{ikr}\left[\sqrt{\pi}\;e^{\pi i/4}\;\;e^{-.076\,kr\,i} - \frac{2.17\,i}{(kr)^{1/2}}\right] \tag{94}$$

$$H_x = \frac{-e^{-\pi i/4}}{\sqrt{\pi}}\,e^{ikr}\left[\sqrt{\pi}\;e^{\pi i/4}\;e^{-.076\,kr\,i} - \frac{2.01\,i}{(kr)^{1/2}}\right] \tag{95}$$

$$H_y = -.831\,i\;\frac{e^{-\pi i/4}\;e^{ikr}}{\sqrt{\pi}\;\;(kr)^{1/2}} \tag{96}$$

$$E_x = E_y = E_z = 0\,. \tag{97}$$

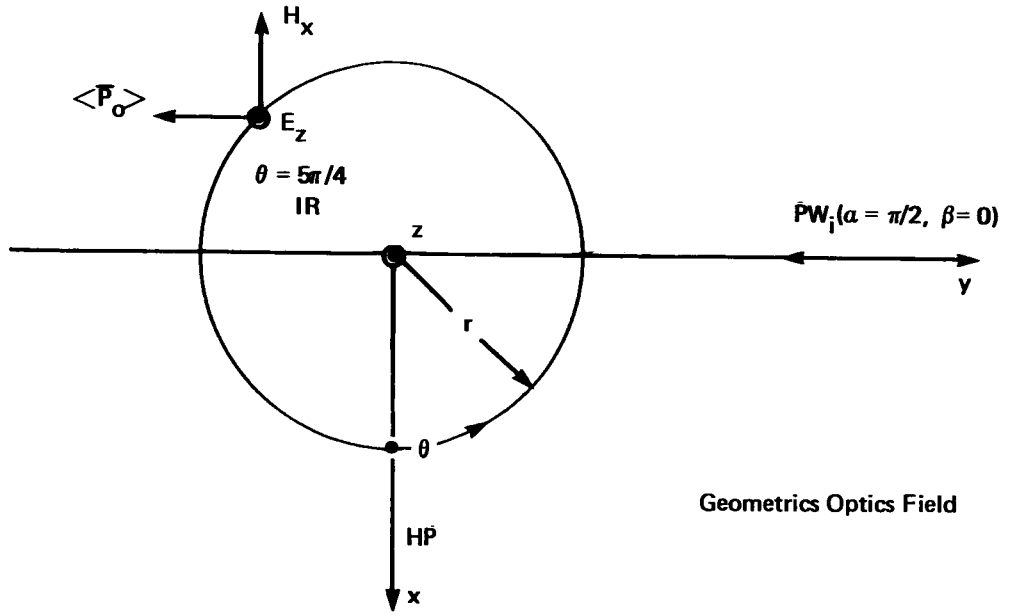

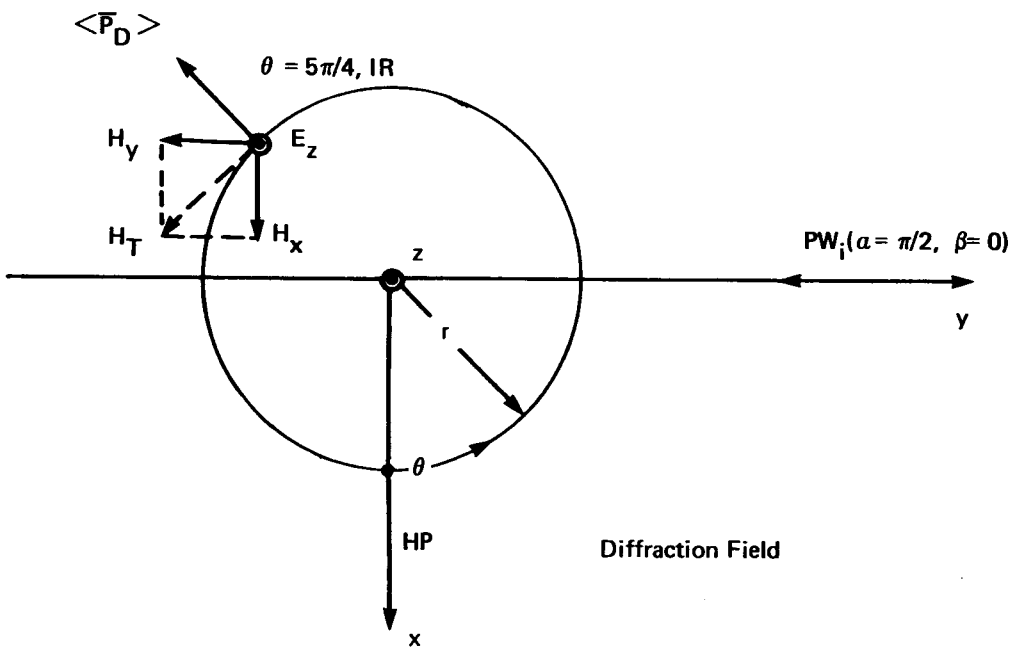

Figure 9. Geometric Optics and Diffraction Fields (E-Plane Polarized)
$\alpha = \pi/2, \beta = 0, \theta = 5\pi/4$

The Poynting vector reduces to

$$<\overline{P}> = \tfrac{1}{2}\,\mathrm{Re}[-\hat{i}\,E_z H_y^* + \hat{j}\,E_z H_x^*] = <\overline{P}_D(r^{-1})> + <\overline{P}_o(r^o)> + <\overline{P}_C(r^{-1/2})>$$

$$= \tfrac{1}{2}\left[\frac{-1.80\,\hat{i}}{\pi kr} - \frac{4.36\,\hat{j}}{\pi kr} - \hat{j}\right] + <\overline{P}_C(r^{-1/2})> \tag{98}$$

and is illustrated in Figure 10.

Figures 9 and 10 tend to show that the diffracted Poynting vector is well-behaved in the IR. Using equations (20) and (21), and defining an angle ξ between $<\overline{P}_D>$ and $-\hat{j}$,

$$\tan\xi = \frac{|H_{yD}|}{|H_{xD}|} = \frac{\left|\frac{-\sin\theta/2}{(kr)^{1/2}}\right|}{\left|\frac{1}{2p} + \frac{1}{2q} + \frac{\cos\theta/2}{(kr)^{1/2}}\right|} = \frac{1}{|\tan\theta|} \tag{99}$$

As θ approaches $3\pi/2$, ξ approaches zero in a continuous manner using equation (99). This implies that the diffracted Poynting vector is everywhere orthogonal to the cylindrical wavefront, contrary to the conclusion reached using the exact solution for G(0).

From equation (74) and Figure 8 it can be seen that H_{yD} does not vanish at the shadow boundary, but tan ξ vanishes due to the fact that $1/p$ is unbounded at θ equals $3\pi/2$. If this singularity is admitted, however, the field quantity H_{xD} is also unbounded, which is an unsatisfactory solution. In conclusion, it appears that a region near the SB is to be avoided when working with the asymptotic solution. Ref. 1, p. 571.

When the observer position is

$$(r, \theta, z) = (r, \pi/2, z) \tag{100}$$

the fixed point lies on the reflection boundary RB and, using Figure 4, $p < 0$, $q = 0$ is anticipated and verified:

$$a = p = -(2kr\cos\beta)^{1/2}\cos\tfrac{1}{2}(\theta - a) = -(2kr)^{1/2} < 0 \tag{101}$$

$$a = q = -(2kr\cos\beta)^{1/2}\cos\tfrac{1}{2}(\theta + a) = 0 \tag{102}$$

Here

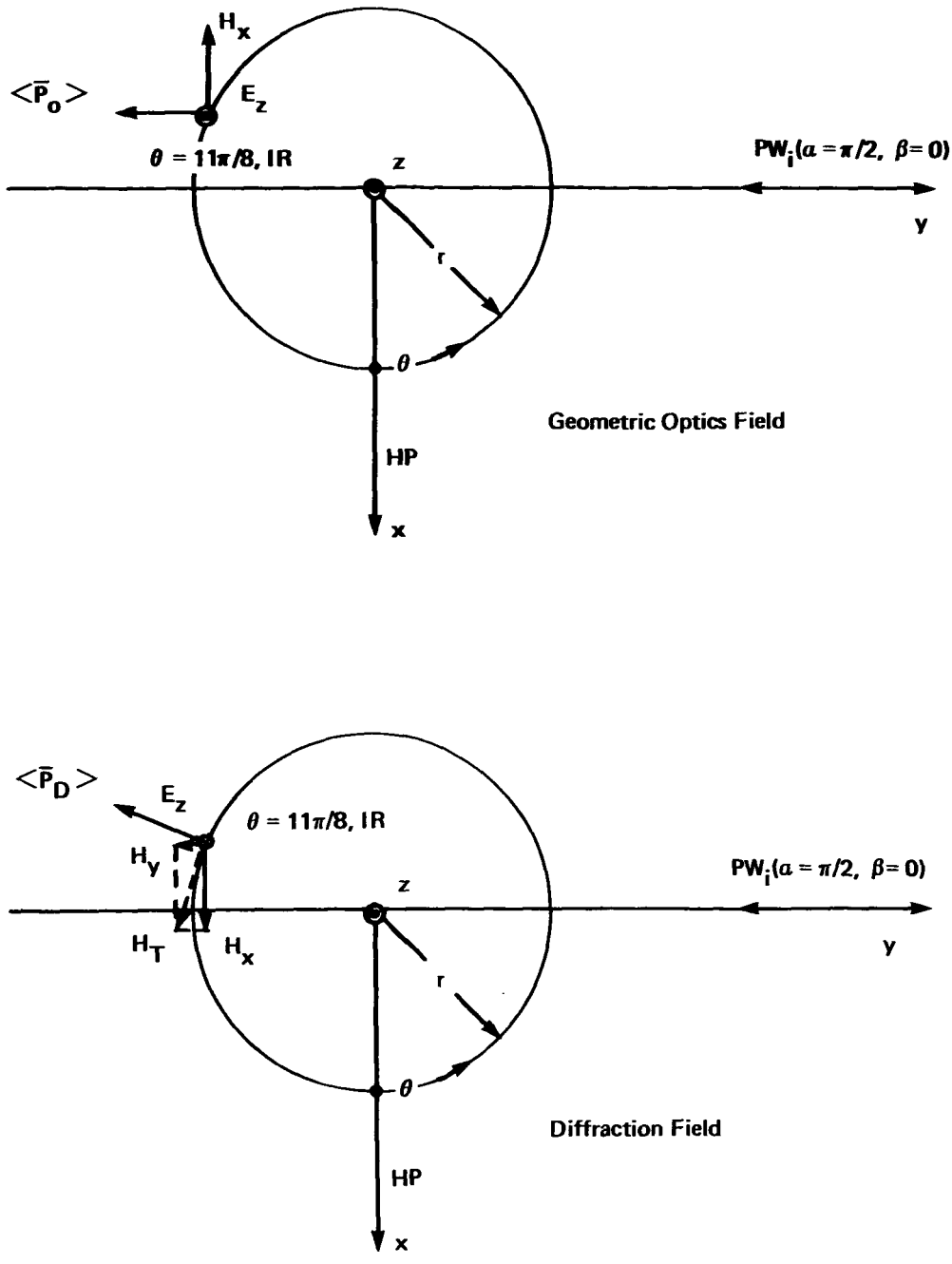

Figure 10. Geometric Optics and Diffraction Fields (E-Plane Polarization)
$\alpha = \pi/2$, $\beta = 0$, $\theta = 11\pi/8$

$$G(p) = \sqrt{\pi}\, e^{\pi i/4}\, e^{-i\,2\,kr} - \frac{i}{2(2kr)^{1/2}} \tag{103}$$

$$G(q) = \tfrac{1}{2}\sqrt{\pi}\, e^{\pi i/4} \tag{104}$$

and

$$E_z = \frac{e^{-\pi i/4}}{\sqrt{\pi}}\, e^{ikr}\left[\sqrt{\pi}\, e^{\pi i/4}\, e^{-i\,2\,kr} - \tfrac{1}{2}\sqrt{\pi}\, e^{\pi i/4} - \frac{i}{2\sqrt{2}\,(kr)^{1/2}}\right] \tag{105}$$

$$H_x = \frac{-e^{-\pi i/4}}{\sqrt{\pi}}\, e^{ikr}\left[\sqrt{\pi}\, e^{\pi i/4} e^{-i\,2\,kr} + \tfrac{1}{2}\sqrt{\pi}\, e^{\pi i/4} + \frac{i}{2\sqrt{2}\,(kr)^{1/2}}\right] \tag{106}$$

$$H_y = \frac{-e^{-\pi i/4}}{\sqrt{\pi}}\, e^{ikr}\left[\frac{i}{\sqrt{2}\,(kr)^{1/2}}\right] \tag{107}$$

$$E_x = E_y = H_z = 0 \tag{108}$$

The Poynting vector reduces to

$$\langle \bar{P} \rangle = \tfrac{1}{2}\,\mathrm{Re}\,[-\hat{i}\,E_z H_y^* + \hat{j}\,E_z H_x^*] = \langle \bar{P}_D(r^{-1}) \rangle + \langle \bar{P}_o(r^o) \rangle + \langle \bar{P}_C(r^{-1/2}) \rangle$$

$$= \tfrac{1}{2}\left[\frac{-\hat{i}}{4\pi kr} + \frac{\hat{j}}{8\pi kr} - \frac{3}{4}\hat{j}\right] + \langle \bar{P}_C(r^{-1/2}) \rangle \tag{109}$$

and is illustrated in Figure 11.

The diffracted Poynting vector $\langle \bar{P}_D \rangle$ is no longer orthogonal to the cylindrical wave front for the present evaluation on the RB even though the exact form of G(q), equation (104), was used. Comments similar to those made for the SB are applicable here.

Although the asymptotic solution leads to a doubtful result on the RB regarding the diffracted wave, the geometrical optics result is once again reliable. From equation (105),

$$E_z(r^o) = e^{-ikr} - \tfrac{1}{2}\, e^{ikr} \tag{110}$$

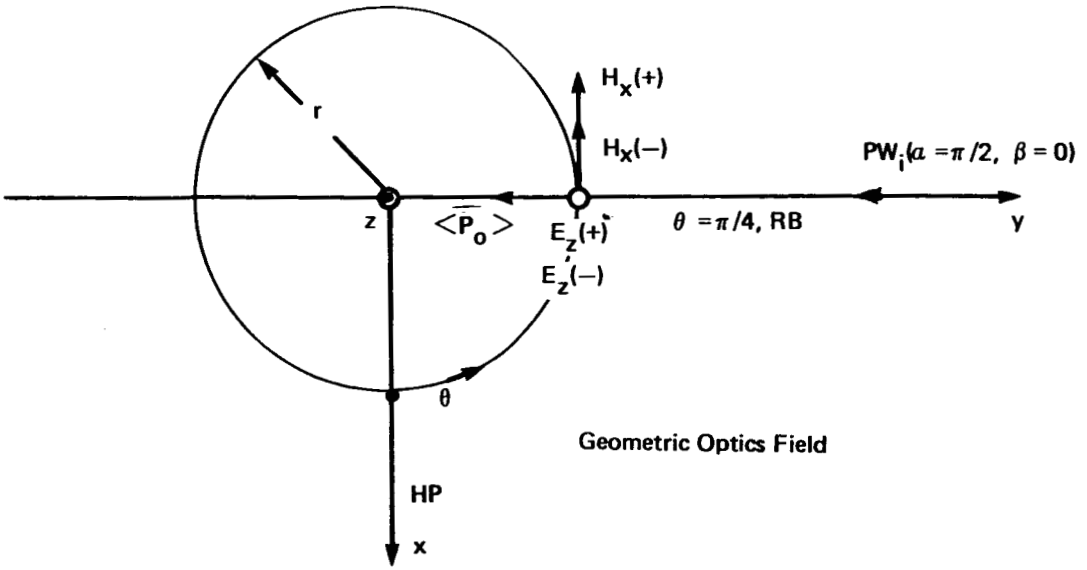

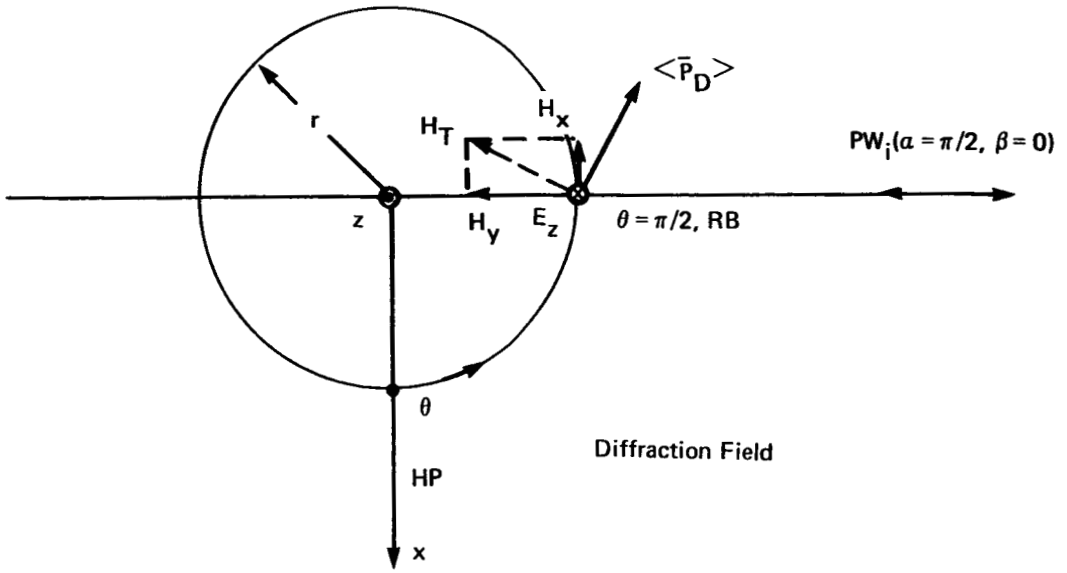

Figure 11. Geometric Optics and Diffraction Fields (E-Plane Polarization)
$\alpha = \pi/2$, $\beta = 0$, $\theta = \pi/2$

which is the arithmetic mean of values on either side of the reflection boundary:

$$\text{A.M.} = \tfrac{1}{2}\left(\underset{RR}{e^{-ikr\cos\beta\cos(\theta-a)}} - \underset{RR}{e^{-ikr\cos\beta\cos(\theta+a)}} + \underset{IR}{e^{-ikr\cos\beta\cos(\theta-a)}}\right). \tag{111}$$

Here the values of a, β, and θ are $\pi/2$,0, and $\pi/2$, respectively.

When the observer position is

$$(r,\theta,z) = (r,0,z) \tag{112}$$

the field point lies on the half-plane and, using Figure 4, $p < 0$, $q < 0$ is anticipated and verified:

$$a = p = -(2kr\cos\beta)^{1/2}\cos\tfrac{1}{2}(\theta - a) = -(kr)^{1/2} < 0 \tag{113}$$

$$a = q = -(2kr\cos\beta)^{1/2}\cos\tfrac{1}{2}(\theta + a) = -(kr)^{1/2} < 0 \tag{114}$$

Here

$$G(p) = G(q) = \sqrt{\pi}\, e^{\pi i/4}\; e^{-ikr} - \frac{i}{2(kr)^{1/2}} \tag{115}$$

and

$$E_z = \frac{e^{-\pi i/4}}{\sqrt{\pi}} e^{ikr}\,[G(p) - G(q)] = 0 \tag{116}$$

$$H_x = \frac{-e^{-\pi i/4}}{\sqrt{\pi}} e^{ikr}\left[G(p) + G(q) + \frac{i}{(kr)^{1/2}}\right] = -2 \tag{117}$$

$$H_y = \frac{e^{-\pi i/4}}{\sqrt{\pi}} e^{ikr}\;[\cos a\, G(p) - \cos a\, G(q) - i\,0] = 0 \tag{118}$$

$$E_x = E_y = H_z = 0 \quad . \tag{119}$$

The Poynting vector reduces to

$$\langle \bar{P} \rangle = \tfrac{1}{2}\,\mathrm{Re}\,[-\hat{i}\,E_z H_y^* + \hat{j}\,E_z H_x^*] = 0 \quad . \tag{120}$$

The preceding solutions indicate that there is no diffracted field component along the half-plane, and reiterate the boundary conditions regarding tangential geometric optics fields. Since $H_x(r^o)$ alone is different from zero the total Poynting vector for θ equal to zero vanishes.

H-PLANE POLARIZATION ($\alpha = \pi/2, \beta = 0$)

The H-plane asymptotic solution is considered for a special case of normal incidence ($\alpha = \pi/2$, $\beta = 0$) with the observer initially at

$$(r, \theta, z) = (r, \pi, 0) \tag{121}$$

under the assumption that

$$kr \cos\beta = kr >> 1 \tag{122}$$

Obviously, the field point lies in the illumination region IR and, using Figure 4, $p<0$, $q>0$ is anticipated and verified:

$$a = p = -(2kr\cos\beta)^{1/2} \cos\tfrac{1}{2}(\theta - \alpha) = -(2kr)^{1/2}\sqrt{2}/2 = -(kr)^{1/2} < 0 \tag{123}$$

$$a = q = -(2kr\cos\beta)^{1/2} \cos\tfrac{1}{2}(\theta + \alpha) = (2kr)^{1/2}\sqrt{2}/2 = (kr)^{1/2} > 0 \quad . \tag{124}$$

Using the preceding arguments in equations (7) and (8),

$$G(p) = \sqrt{\pi}\, e^{\pi i/4} e^{-ikr} - \frac{i}{2(kr)^{1/2}} \tag{125}$$

and

$$G(q) = \frac{i}{2(kr)^{1/2}} \tag{126}$$

The geometric optics and diffraction fields may now be identified for equations (23) through (28).

$$E_x = \frac{e^{-\pi i/4}}{\sqrt{\pi}} e^{ikr}\left[\sqrt{\pi}\, e^{\pi i/4}\, e^{-ikr} - \frac{i}{2(kr)^{1/2}} - \frac{i}{2(kr)^{1/2}} \oplus i\left(\frac{2}{kr}\right)^{1/2}\frac{\sqrt{2}}{2}\right] = 1 \tag{127}$$

$$H_z = 1 \tag{128}$$

$$E_y = E_z = H_x = H_y = 0 \quad . \tag{129}$$

The time-average Poynting vector, using the total fields, reduces to

$$\begin{aligned} \langle \bar{P} \rangle &= \tfrac{1}{2}\,\mathrm{Re}\,[-\hat{j}\, E_x H_z^*] = \langle \bar{P}_D(r^{-1}) \rangle + \langle \bar{P}_o(r^o) \rangle + \langle \bar{P}_C(r^{-1/2}) \rangle \\ &= \tfrac{1}{2}[-\hat{j}] + 0\ \langle \bar{P}_D(r^{-1}) \rangle + 0\ \langle \bar{P}_C(r^{-1/2}) \rangle \ . \end{aligned} \tag{130}$$

A null in the diffraction field is indicated. More importantly, the $\oplus$ sign of equation (127) appears to be correct since the opposite sign would lead to a diffracted (cylindrical) component E_x without a magnetic counterpart. This result is not taken as conclusive, however, since the diffracted Poynting vector vanished in the present example.

When the observer position is

$$(r, \theta, z) = (r, 5\pi/4, z) \tag{131}$$

the field point lies in the illumination region, and using Figure 4, $p<0$, $q>0$ is anticipated and verified:

$$a = p = -(2kr\cos\beta)^{1/2}\cos^{1/2}(\theta - \alpha) = -.541(kr)^{1/2} < 0 \tag{132}$$

$$a = q = -(2kr\cos\beta)^{1/2}\cos^{1/2}(\theta + \alpha) = 1.31(kr)^{1/2} > 0 \tag{133}$$

Here

$$G(p) = \sqrt{\pi}\, e^{\pi i/4}\, e^{-.293\, kri} - \frac{.924\, i}{(kr)^{1/2}} \tag{134}$$

$$G(q) = \frac{.383\, i}{(kr)^{1/2}} \tag{135}$$

and

$$E_x = \frac{e^{-\pi i/4}}{\sqrt{\pi}}\, e^{ikr}\left[\sqrt{\pi}\, e^{\pi i/4}\, e^{-.293\, kri} - \frac{.924i}{(kr)^{1/2}} - \frac{.383\, i}{(kr)^{1/2}} \oplus \left(\frac{2}{kr}\right)^{1/2}\frac{\sqrt{2}}{2}(.924)\, i\right]$$

$$= \frac{e^{-\pi\, i/4}}{\sqrt{\pi}}\, e^{ikr}\left[\sqrt{\pi}\, e^{\pi i/4}\, e^{-.293\, kri} - \frac{.383\, i}{(kr)^{1/2}}\right] \tag{136}$$

$$E_y = \frac{-e^{-\pi\, i/4}}{\sqrt{\pi}}\, e^{ikr}\left[\oplus\, i\left(\frac{2}{kr}\right)^{1/2}\frac{\sqrt{2}}{2}(-.383)\right] = \frac{.383\, e^{-\pi\, i/4}\, e^{ikr}\, i}{\sqrt{\pi}\,(kr)^{1/2}} \tag{137}$$

$$H_z = \frac{e^{-\pi i/4}}{\sqrt{\pi}}\, e^{ikr}\left[\sqrt{\pi}\, e^{\pi\, i/4}\, e^{-.293\, kri} - \frac{.541\, i}{(kr)^{1/2}}\right] \tag{138}$$

$$E_z = H_x = H_y = 0. \tag{139}$$

The Poynting vector reduces to

$$<\bar{P}> = \tfrac{1}{2}\,\mathrm{Re}\,[\hat{i}\,E_y H_z^* - \hat{j}\,E_x H_z^*] = <\bar{P}_D(r^{-1})> + <\bar{P}_o(r^o)> + <\bar{P}_C\,(r^{-1/2})>$$

$$= \tfrac{1}{2}\left[\frac{-.206\hat{i}}{\pi\,kr} - \frac{.207\hat{j}}{\pi\,kr} - \hat{j}\right] + <\bar{P}_C\,(r^{-1/2})> \qquad (140)$$

and is illustrated in Figure 12.

Figure 12 shows that the diffracted Poynting vector $<\bar{P}_D>$ is orthogonal to the cylindrical wavefront in the selected point of the IR using the $\oplus$ sign for both equations (23) and (24). This reinforces the indication of the previous example for θ equals π radians, and the derivation of TM 84996. The consequences of using the $\ominus$ sign for both equations, Ref. 1, 2nd Edition, are given below, and are illustrated in Figure 13. Similarly, the consequences of using the $\ominus$ sign for equation (23) and the $\oplus$ sign for equation (24), Ref. 1, 6th Edition, are given below, and are illustrated in Figure 14. It can be seen that the diffracted Poynting vector $<\bar{P}_D>$ is not orthogonal to the wavefront for a point, θ equals $5\pi/4$ radians, deep in the illumination region IR for the latter two examples. The $\oplus$ sign will therefore be applied to equations (22) and (23) of TM 84996 and equations (23) and (24) of TM 86221 as indicated.

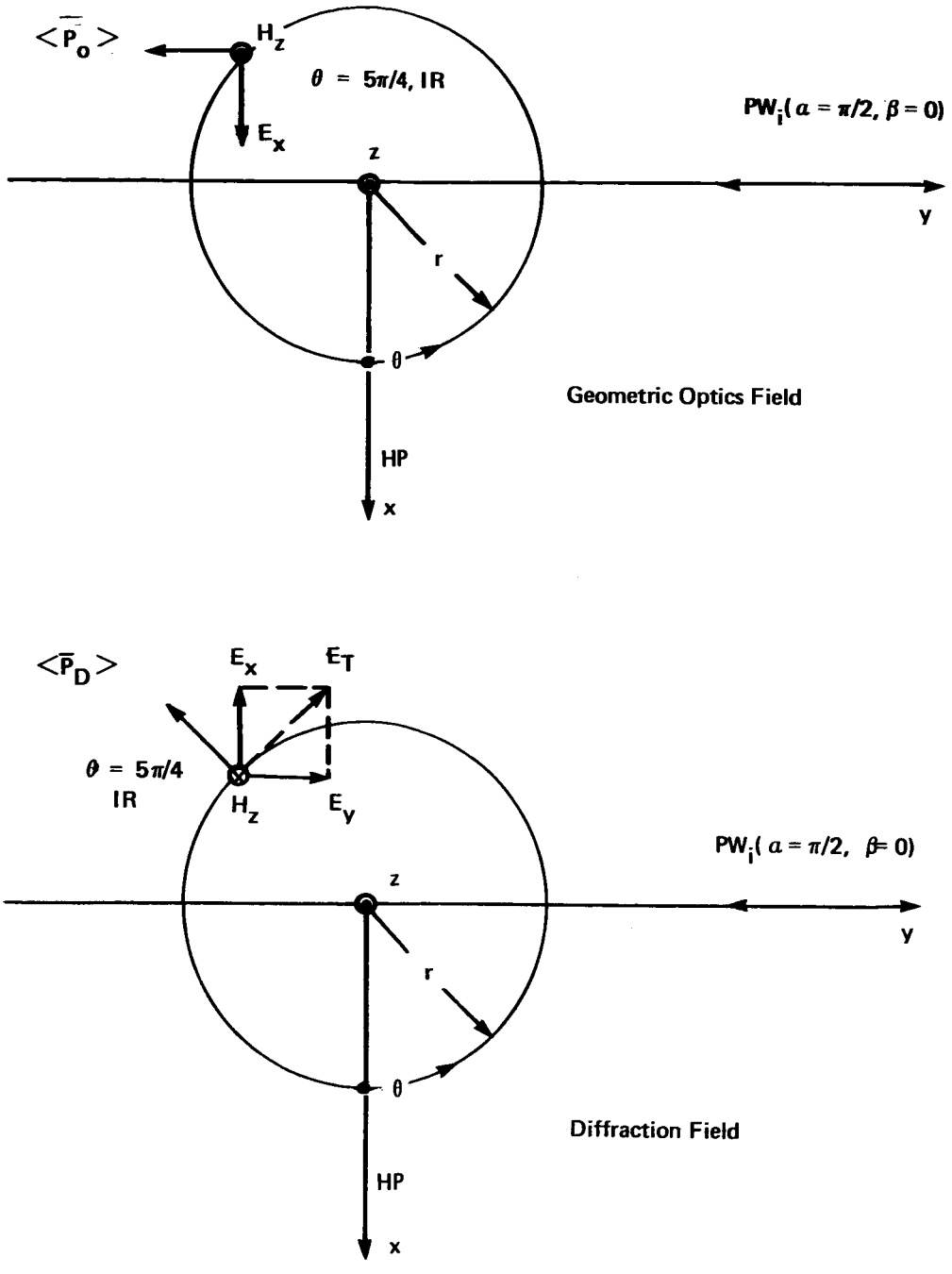

Figure 12. Geometric Optics and Diffraction Fields (H-Plane Polarization)
$\alpha = \pi/2$, $\beta = 0$, $\theta = 5\pi/4$
Signs: ⊖ , ⊕ of TM 84996

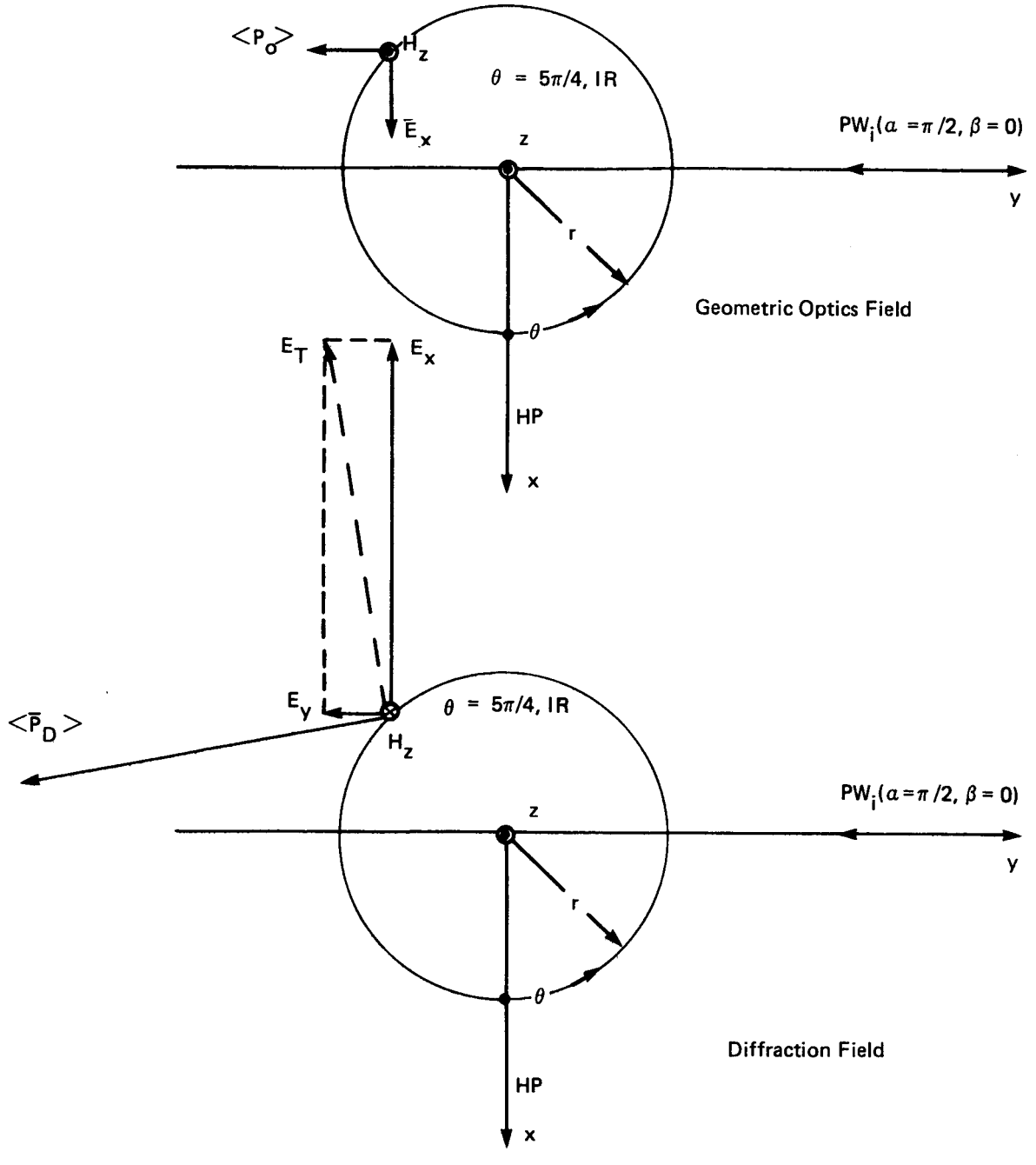

Figure 13. Geometric Optics and Diffraction Fields (H-Plane Polarization)
$\alpha = \pi/2$, $\beta = 0$, $\theta = 5\pi/4$
Signs: ⊖ , ⊖ of Ref. 1, 2nd Edition

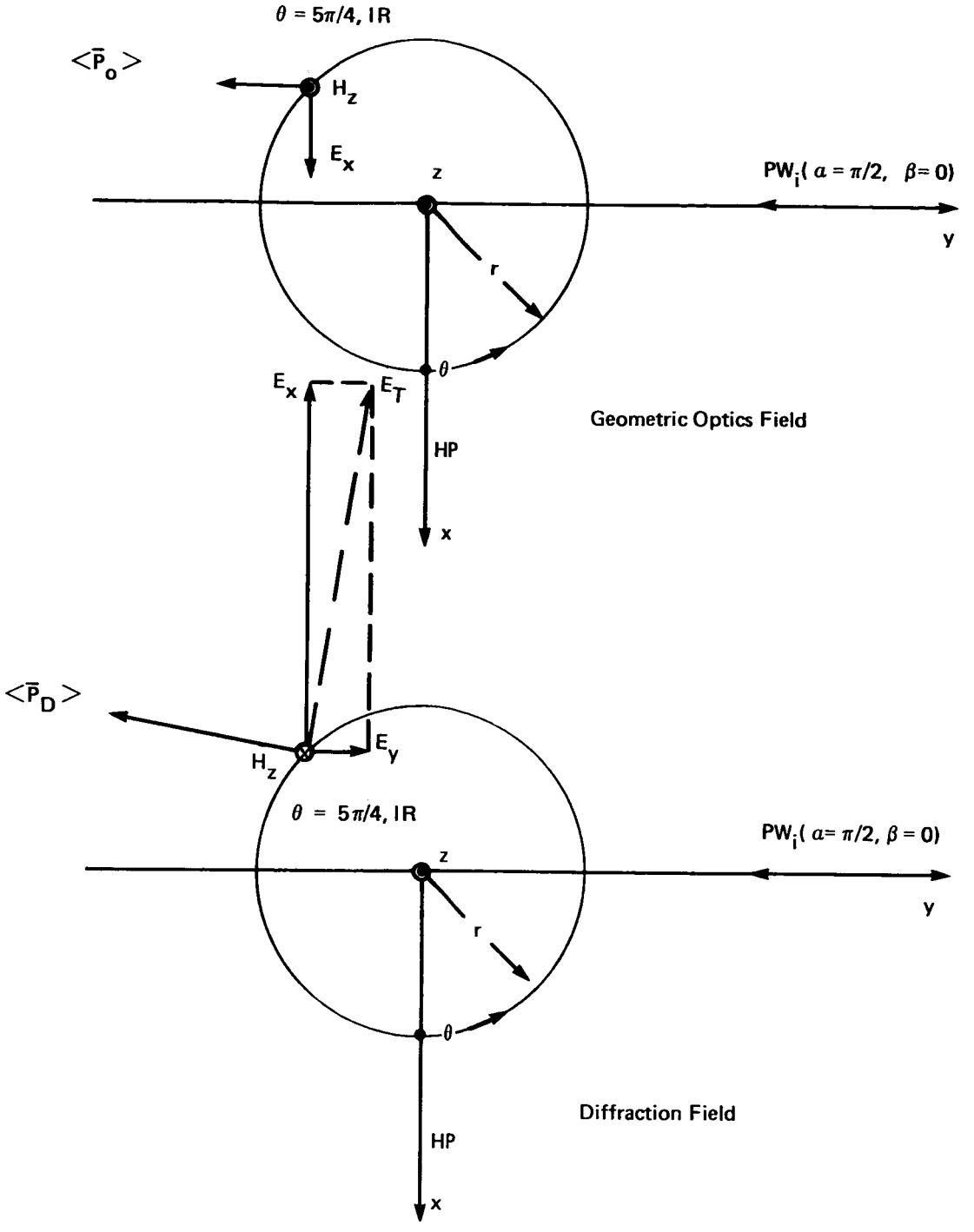

Figure 14. Geometric Optics and Diffraction Fields (H-Plane Polarization)
$\alpha = \pi/2$, $\beta = 0$, $\theta = 5\pi/4$
Signs: ⊖ , ⊕ of Ref. 1, 6th Edition

Ref. 1, 2nd Edition signs:

$$E_x = \frac{e^{-\pi i/4}}{\sqrt{\pi}} e^{ikr}\left[\sqrt{\pi}\, e^{\pi i/4}\, e^{-.293\, kri} - \frac{.924\, i}{(kr)^{1/2}} - \frac{.383\, i}{(kr)^{1/2}} \ominus \left(\frac{2}{kr}\right)^{1/2}\frac{\sqrt{2}}{2}(.924)i\right]$$

$$= \frac{e^{-\pi i/4}}{\sqrt{\pi}} e^{ikr}\left[\sqrt{\pi}\, e^{\pi i/4}\, e^{-.293\, kri} - \frac{2.231\, i}{(kr)^{1/2}}\right] \qquad (141)$$

$$E_y = \frac{-e^{-\pi i/4}}{\sqrt{\pi}} e^{ikr}\left[\ominus\, i\left(\frac{2}{kr}\right)^{1/2}\frac{\sqrt{2}}{2}(-.383)\right] = \frac{-.383\, e^{-\pi i/4}\, e^{ikr}}{\sqrt{\pi}\,(kr)^{1/2}}\, i \qquad (142)$$

$$H_z = \frac{e^{-\pi i/4}}{\sqrt{\pi}} e^{ikr}\left[\sqrt{\pi}\, e^{\pi i/4}\, e^{-.293\, kri} - \frac{.541\, i}{(kr)^{1/2}}\right] \qquad (143)$$

$$E_z = H_x = H_y = 0 \quad . \qquad (144)$$

The Poynting vector reduces to

$$\langle \bar{P} \rangle = \tfrac{1}{2}\, \mathrm{Re}\,[\, \hat{i}\, E_y H_z^* - \hat{j}\, E_x H_z^*] = \langle \bar{P}_D\, (r^{-1}) \rangle + \langle \bar{P}_o (r^o) \rangle + \langle \bar{P}_C\, (r^{-1/2}) \rangle$$

$$= \tfrac{1}{2}\left[\frac{.207\, \hat{i}}{\pi kr} - \frac{1.21\, \hat{j}}{\pi\, kr} - \hat{j}\right] + \langle \bar{P}_C\, (r^{-1/2}) \rangle \qquad (145)$$

and is illustrated in Figure 13.

Ref. 1, 6th Edition signs:

$$E_x = \frac{e^{-\pi i/4}}{\sqrt{\pi}}\ e^{ikr}\left[\sqrt{\pi}\ e^{\pi i/4}\ e^{-.293\ kri} - \frac{.924\ i}{(kr)^{1/2}} - \frac{.383\ i}{(kr)^{1/2}} \ominus \left(\frac{2}{kr}\right)^{1/2}\frac{\sqrt{2}}{2}(.924)\ i\right]$$

$$= \frac{e^{-\pi i/4}}{\sqrt{\pi}}\ e^{ikr}\left[\sqrt{\pi}\ e^{\pi\ i/4}\ e^{-.293\ kri} - \frac{2.231\ i}{(kr)^{1/2}}\right] \qquad (146)$$

$$E_y = \frac{-e^{-\pi i/4}}{\sqrt{\pi}} e^{ikr}\left[\oplus\ i\left(\frac{2}{kr}\right)^{1/2}\frac{\sqrt{2}}{2}(-.383)\right] = \frac{.383\ e^{-\pi i/4}\ e^{ikr}}{\sqrt{\pi}\ (kr)^{1/2}}\ i \qquad (147)$$

$$H_z = \frac{e^{-\pi i/4}}{\sqrt{\pi}}\ e^{ikr}\left[\sqrt{\pi}\ e^{\pi i/4}\ e^{-.293\ kri} - \frac{.541\ i}{(kr)^{1/2}}\right] \qquad (148)$$

$$E_z = H_x = H_y = 0 \quad . \qquad (149)$$

The Poynting vector reduces to

$$\langle \bar{P} \rangle = \tfrac{1}{2}\,\mathrm{Re}\,[\hat{i}\,E_y H_z^* - \hat{j}\,E_x H_z^*] = \langle \bar{P}_D(r^{-1}) \rangle + \langle \bar{P}_o(r^o) \rangle + \langle \bar{P}_C(r^{-1/2}) \rangle$$

$$= \tfrac{1}{2}\left[\frac{-2.07\ \hat{i}}{\pi\ kr} - \frac{1.21\ \hat{j}}{\pi\ kr}\right] \qquad (150)$$

and is illustrated in Figure 14.

E-PLANE POLARIZATION ($\alpha = \pi/2, \beta \neq 0$)

The E-plane asymptotic solution is considered for a special set of cases of oblique incidence ($\alpha = \pi/2, \beta \neq 0$) with the observer at

$$(r, \theta, z) = (r, \pi, 0) \tag{151}$$

under the assumption that

$$kr \cos\beta >> 1 \quad . \tag{152}$$

Figure 15 shows that the field point lies in the illumination region IR and, using Figure 4, $p < 0$, $q > 0$ is anticipated and verified:

$$a = p = -(2kr \cos\beta)^{1/2} \cos 1/2(\theta - \alpha) = -(kr \cos\beta)^{1/2} \tag{153}$$

$$a = q = -(2kr \cos\beta)^{1/2} \cos 1/2(\theta + \alpha) = (kr \cos\beta)^{1/2} \quad . \tag{154}$$

Using the preceding arguments in equations (7) and (8),

$$G(p) = \sqrt{\pi}\, e^{\pi i/4}\, e^{-ikr \cos\beta} - \frac{i}{2(kr \cos\beta)^{1/2}} \tag{155}$$

and

$$G(q) = \frac{i}{2(kr \cos\beta)^{1/2}} \quad . \tag{156}$$

The geometric optics and diffraction fields may now be identified for equations (17) through (22).

$$E_z = \cos\beta\, e^{-ik\, z \sin\beta} - i\, \frac{e^{-\pi i/4}}{\sqrt{\pi}}\, \frac{\cos\beta\, e^{ik(r \cos\beta - z \sin\beta)}}{(kr \cos\beta)^{1/2}} \tag{157}$$

$$H_x = -e^{-ikz \sin\beta} \tag{158}$$

$$H_y = \frac{-i}{\sqrt{\pi}}\, \frac{e^{-\pi i/4}\, e^{ik(r\cos\beta - z \sin\beta)}}{(kr \cos\beta)^{1/2}} \tag{159}$$

$$E_x = -H_y \sin\beta \tag{160}$$

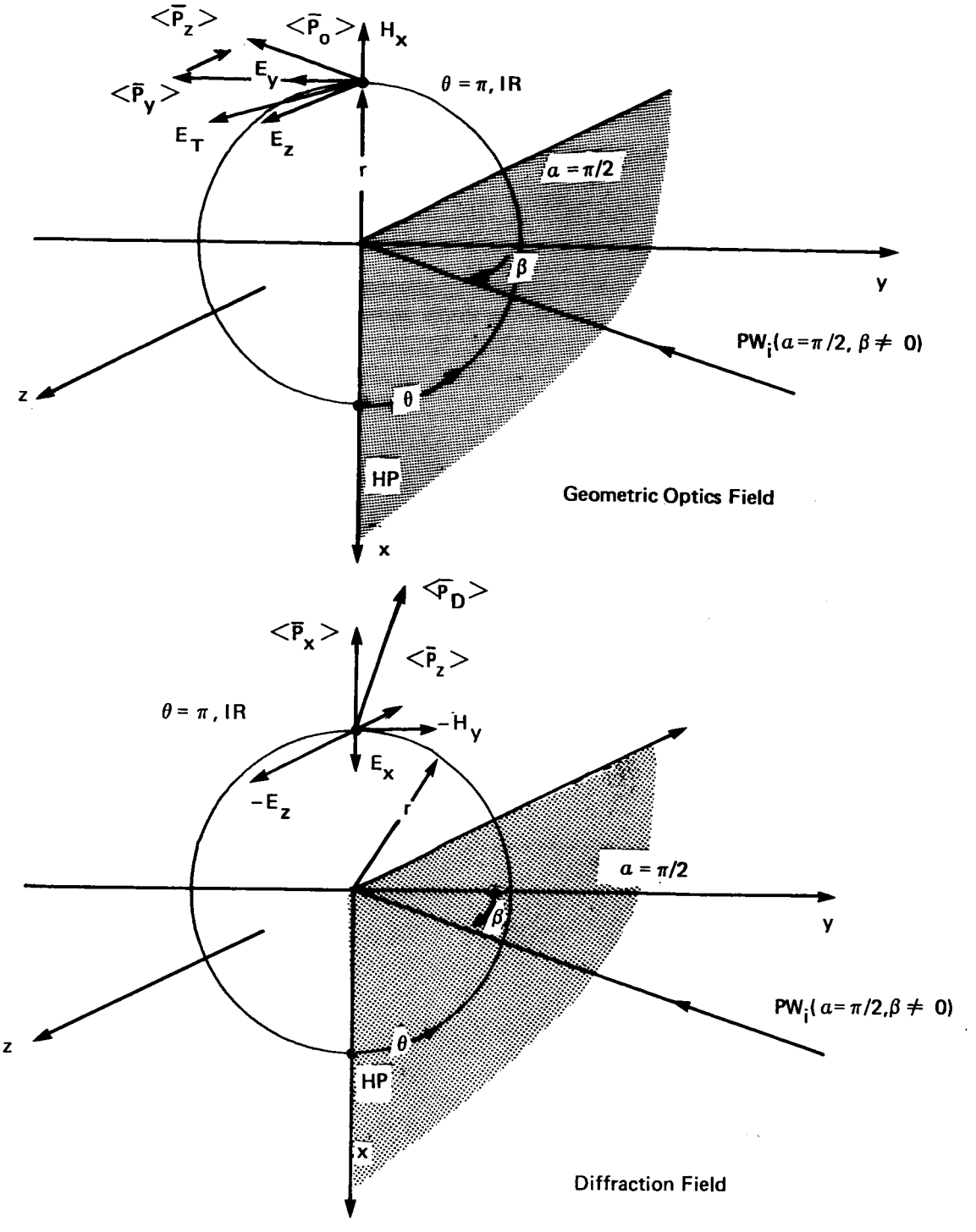

Figure 15. Geometric Optics and Diffraction Fields (E-Plane Polarized)
$a = \pi/2$, $\beta \neq 0$, $\theta = \pi$

$$E_y = H_x \sin\beta \tag{161}$$

$$H_z = 0 \ . \tag{162}$$

The time average Poynting vector, using the total fields, is

$$\langle \bar{P} \rangle = \tfrac{1}{2} \mathrm{Re}\, \bar{E} \times \bar{H}^* = \tfrac{1}{2} \mathrm{Re} \left[\hat{i}\,(E_y H_z^* - E_z H_y^*) + \hat{j}\,(E_z H_x^* - E_x H_z^*) + \hat{k}\,(E_x H_y^* - E_y H_x^*) \right] \tag{163}$$

which reduces to

$$\langle \bar{P} \rangle = \tfrac{1}{2} \mathrm{Re}\, [\, -\hat{i}\, E_z H_y^* + \hat{j}\, E_z H_x^* + \hat{k}\,(E_x H_y^* - E_y H_x^*)]$$

$$= \langle \bar{P}_D(r^{-1}) \rangle + \langle \bar{P}_o(r^o) \rangle + \langle \bar{P}_C\,(r^{-1/2}) \rangle$$

$$= \tfrac{1}{2} \left[\frac{-\hat{i} \cos\beta - \hat{k} \sin\beta}{\pi kr \cos\beta} \quad -\hat{j} \cos\beta - \hat{k} \sin\beta \right] + \langle \bar{P}_C(r^{-1/2}) \rangle \tag{164}$$

subject to equation (152), and is illustrated in Figure 15. Equation (164) degenerates to equation (40) under β equals zero.

Equation (164) shows the Poynting vectors $\langle \bar{P}(r^o) \rangle$ amd $\langle \bar{P}(r^{-1}) \rangle$ associated with the geometric optics and diffracted fields, respectively, for an incident plane wave with angle α equal to $\pi/2$ radians, and β arbitrary. The diffracted power density $\langle \bar{P}(r^{-1}) \rangle$ diverges as r^{-1} since the electric and magnetic fields diverge as $r^{-1/2}$. This indicates a cylindrical wave, regarding the diffracted fields independently, for which total power is conserved as it passes through concentric cones:

$$\iint_c \langle \bar{P}(r^{-1}) \rangle \cdot d\bar{S} = \text{constant} \tag{165}$$

Here

$$\iint_c dS = \iint_c r\, d\theta\, dh_s = \iint_c \frac{r\, d\theta\, dr}{\sin\xi} = \pi r h_s \tag{166}$$

for a cone of slant height h_s and half-angle ξ, but it remains to show that

$$\langle \bar{P}_u(r^{-1}) \rangle \cdot \bar{n}_c = 1 \tag{167}$$

for the present example when $\langle \bar{P}_u \rangle$ is a unit vector.

Figure 16 illustrates the separate arguments of an exponential term (phase factor) of the magnetic field of equation (159), and the combined argument, about the diffracting edge. Setting this phase term equal to a constant, the wavefront Λ is obtained and the components of the corresponding normal $\bar{n}_\Lambda$ are given by

$$\bar{n}_c = \bar{n}_\Lambda = (\cos\beta\cos\theta, \cos\beta\sin\theta, -\sin\beta) \quad . \tag{168}$$

In Figure 16, θ equals π radians is illustrated, and

$$<\bar{P}_u(r^{-1})> \bullet \bar{n}_c = (-\hat{i}\cos\beta - \hat{k}\sin\beta) \bullet (-\hat{i}\cos\beta - \hat{k}\sin\beta) = 1 \tag{169}$$

is established for the present example.

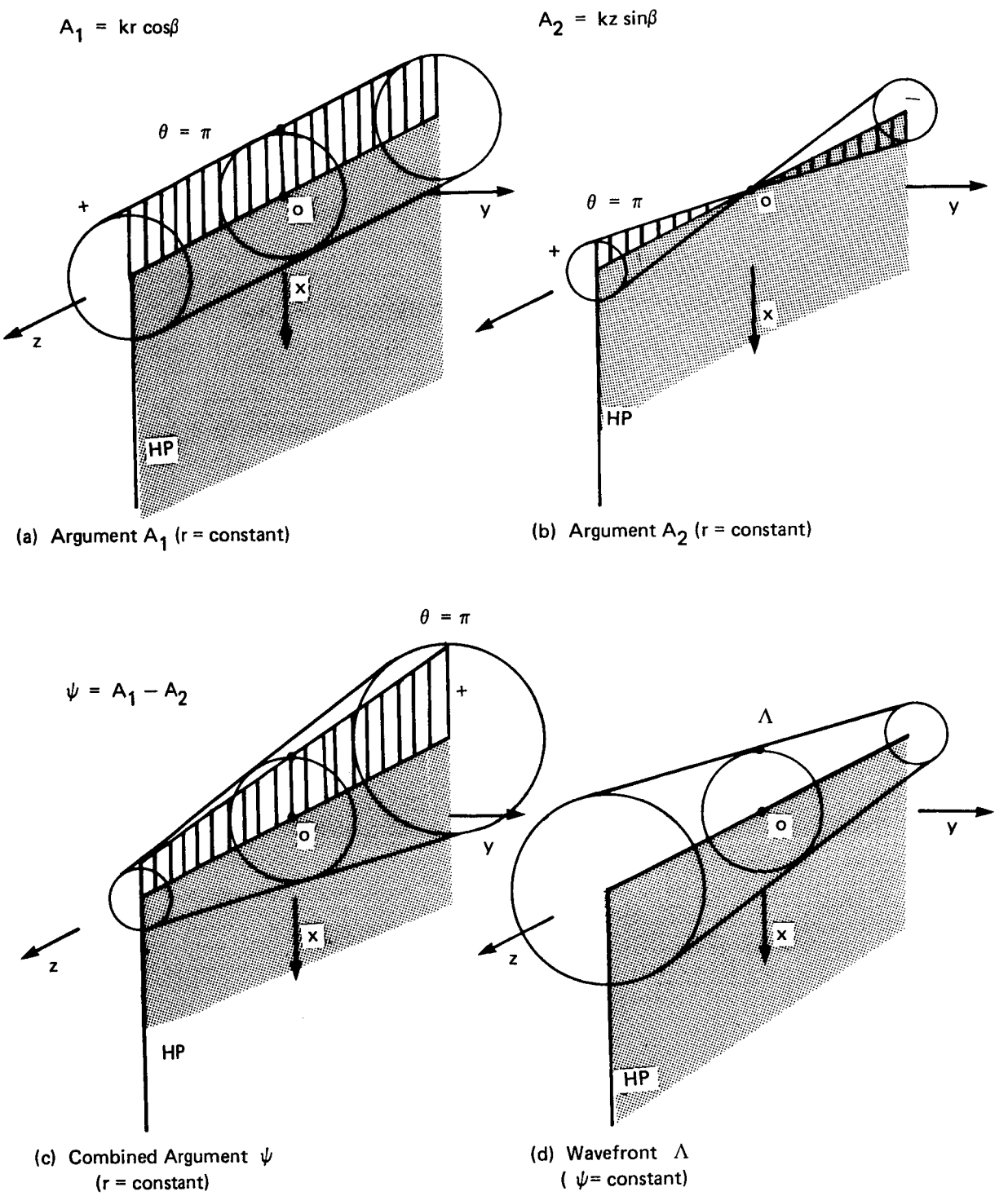

Figure 16. Evolution of the Cylindrical Wavefront for Oblique Incidence
$\alpha = \pi/2$, $\beta \neq 0$, $\theta = \pi$

DIFFRACTING HALF-PLANES OF FINITE LENGTH

In TM 84996 the classical solution for scattering from a half-plane was proposed for dealing with fences of finite length to determine the perturbation on the effective radiation pattern of paraboloidal antennas. Aside from possible multiple interaction between members of a polygonal fence, the application of the half-plane solution for even a single fence may be inappropriate for other reasons. An examination of the geometrical parameters of a proposed security fence installation at the Merritt Island, FL Spacecraft Tracking and Data Network Station showed that lengths of 60, 70, 130, and 140 feet would be encountered. The distances R to the shortest and longest fences are approximately 64 and 56 feet, respectively, from the center of the antenna base.

An attempt is now made to determine whether or not the assumption of the fields scattered from an infinitely-long conducting half-plane is reasonably valid for the 60 and 140 foot fences at S and Ku band. From Figure 17 it can be seen that, for a fence of finite length L, there is a fraction ℓ of its length which appears phase-stationary in some sense as seen from a point of observation. The pad center is arbitrarily selected as that point here, and the criterion of stationarity is taken to be a numeric N (equal to δ/λ).

$$(R + \delta)^2 = R^2 + (\ell/2)^2 \tag{170}$$

$$\ell \doteq (8\,NR\,\lambda)^{1/2} \tag{171}$$

If phase quadrature is taken as the criterion N equals one-fourth, the regions of the fence which appear stationary in the present context may be calculated at S-band (λ = 1/2 ft.) and Ku-band (λ= 1/12 ft.) for the fence lenghts L and associated distances R. The results are given in Figure 17.

An interpretation of the results is that a fraction ℓ/L of a finite fence may be stationary, but that ratio is equal to zero for an infinite fence which gives rise to cylindrical wave. The greater the ratio of ℓ /L, therefore, the weaker the justification for the present half-plane analysis. Alternatively, for a finite fence there exists some distance R, sufficiently large, so that the entire fence is essentially stationary and the radiation observed no longer diverges as a cylindrical wave, but like that of a point source or spherical wave. The quadrature stationarity criterion

$$N = \delta/\lambda = \tfrac{1}{4} \tag{172}$$

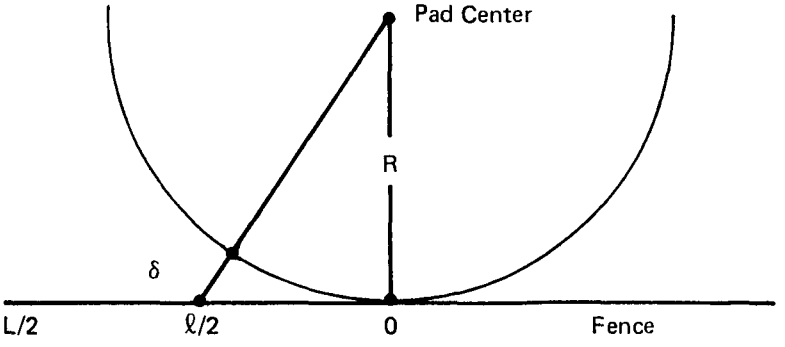

L = 60 feet, R = 64 feet, N = 1/4
ℓ = 8.0 feet (S-Band)
ℓ = 3.3 feet (Ku-Band)

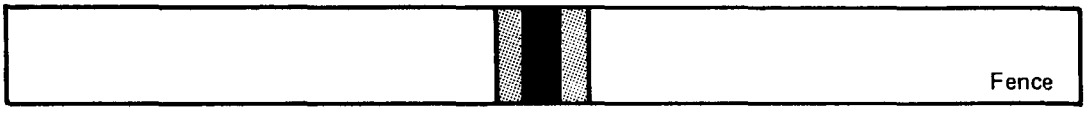

L = 140 feet, R = 56 feet, N = 1/4
ℓ = 11.8 feet (S-Band)
ℓ = 4.8 feet (Ku-Band)

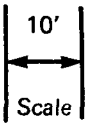

Figure 17. Stationary Sectors of Finite-Length Fences

used to obtain Figure 17 regards a very weak stationarity and should be compared to the criterion

$$N = 1/16 \tag{173}$$

that is applied in the manufacture of paraboloidal reflectors of ordinary industrial quality.

The half-plane analysis discussed in this technical memorandum will not be applicable to represent the physical installation at Merritt Island, FL at Ku-band. There is no problem regarding stationarity and, as shown by Figure 17, a Ku-band simulation is easier to justify than one at S-band for the fence lengths and observer distances noted. The difficulty lies with the mesh size of the fences. At S-band the approximately 2.5 x 2.5-inch mesh appears to be an essentially continuous, perfectly conducting half-plane segment. At Ku-band the same mesh appears to be a doubly periodic structure or filter with a calculable transmission and reflection coefficient that depends, in general, on the angle of incidence and polarization orientation.

CONCLUSION

In this technical memorandum, a sequel to TM 84996, the propagation mechanics of the diffracting half-plane have been explored using an asymptotic solution. Certain sign discrepancies in the field equations were resolved by an independent derivation of those equations and a graphical examination of the diffracted fields and the associated time-average Poynting vectors. The asymptotic solution was applied for points of observation in the shadow, illumination, and reflection regions according to ascending complexity, and geometric optics fields were separated from the diffraction fields. A similar application of the asymptotic solution was made on the shadow and reflection boundaries, anticipating some difficulties. It was found that the geometric optics solutions were reliable, and the transition across these boundaries lead to the recovery of the arithmetic mean for the field quantities. The diffracted fields on these boundaries are deemed to be unreliable, leading to Poynting vectors that are not orthogonal to a cylindrical wavefront.

The case of general incidence (α , β) was explored in order to answer questions concerning singularities triggered by the $\cos\beta$ term and the shape of the diffracted-field wavefront. The time-average Poynting vector was separated according to the divergence (r^{-1}, r^{0}, $r^{-1/2}$) that resulted from considering the total magnetic and electric field quantities of the asymptotic solution. These diverged as (r^{0}, $r^{-1/2}$), and gave rise to cross-product terms in the development of the Poynting vectors. It was found that the diffracted wavefront is a conical cylinder for general incidence, and degenerates to right-circular cylinder for orthogonal incidence. Further, the law of divergence for the diffracted wave taken independently is compatible with the area of concentric conical wavefronts in the sense that energy conservation is preserved.

Returning to the more immediate concern, the diffraction fences at Merritt Island, FL, it was concluded that the formulation involving the Fresnel integrals could be by-passed since the perturbation from a fence resides entirely in the diffracted magnetic fields of the Sommerfeld asymptotic solution for the fence geometry presented at this time. An exploration of the phase stationarity at S and Ku-bands disclosed that the Sommerfeld solution would not be applicable if the fences were significantly further from the paraboloidal antenna base. (In any event, modal analysis will be required at Ku-band due to the doubly-periodic mesh of the fence.) It is unlikely that fences would ever be in such close proximity to the antenna as to require Fresnel integration, and also unlikely that the reflection region would have to be considered. Present plans include the mapping of those convoluted fields for large distances from the diffracting half-plane edge.

ACKNOWLEDGEMENTS

This document is based on the Sommerfeld half-plane solution found in "Principles of Optics," by M. Born and E. Wolf. The author is indebted to R. Meneghini of the Laboratory for Oceans, GSFC and to Dr. M. Kao of Science Applications Research for in-depth discussions and critical review. The financial support obtained from the Telecommunications System Branch, GSFC, via H. O'Donnell is also gratefully acknowledged.

REFERENCES

1. Born, M. and Wolf, E., "Principles of Optics," 2nd Edition, Pergamon Press, 1964.

APPENDIX A

ERRATA TO TM 84996

The following errors have been detected.

Page 6, equation (16)

Replace cos $\theta/2$ with sin $\theta/2$

Page 7, equation (27)

Multiply the right-hand side of (27) by cos β

Page 8, one line above equation (29)

Replace "same" with "some"

Page 17, two lines above equation (62)

Replace "respec" with "respect"

Page A-1, one line below equation (1-A)

Multiply the right-hand side of the equation for C by $e^{-ik\,z\,\sin\beta}$, and delete i in the equation for E.

Page B-2, below equation (10-B)

Replace p. 76 with p. 573 .

1. Report No.	2. Government Accession No.	3. Recipient's Catalog No.
TM 86221		

4. Title and Subtitle	5. Report Date
Three-Dimensional Diffraction of a Plane Wave by a Half-plane	June 1985
	6. Performing Organization Code
7. Author(s)	8. Performing Organization Report No.
R. F. Schmidt	
	10. Work Unit No.
9. Performing Organization Name and Address	11. Contract or Grant No.
National Aeronautics & Space Administration Goddard Space Flight Center Greenbelt, MD 20771	
	13. Type of Report and Period Covered
12. Sponsoring Agency Name and Address	Technical Memorandum
National Aeronautics & Space Administration Washington, DC 20546	14. Sponsoring Agency Code

15. Supplementary Notes

16. Abstract

This document discusses several aspects of the asymptotic Sommerfeld solutions for a diffracting half-plane. The behavior of the E-plane and H-plane solutions for general (two angleparameter) incidence is explored in the remote shadow, reflection, and illumination regions using the time-average Poynting vector. Field points are also taken on the shadow and reflection boundaries to characterize the behavior of the asymptotic solutions in these special regions. Geometric-optics field transition between adjacent sectors via the arithmetic mean is verified. Numerous sketches are included to assist visualization of the content of the three-dimensional Sommerfeld solutions and clarify some of the notation and conventions introduced in TM 84996 of March 1983. The closed-form field equations discussed in this document provide an analytical basis for comparison with the numerical results of a computer program predicated on the less-restrictive Fresnel-integral approach.

17. Key Words (Suggested by Author(s))	18. Distribution Statement
	Unclassified–Unlimited

19. Security Classif. (of this report)	20. Security Classif. (of this page)	21. No. of Pages	22. Price
Unclassified	Unclassified	49	

N-305 For sale by the National Technical Information Service, Springfield, Virginia 22161